Asynchronous dynamics of the last Scandinavian Ice Sheet along the Pomeranian Phase ice-marginal belt: a new scenario inferred from surface exposure $^{10}$Be dating

Karol Tylmann[1*], Vincent R. Rinterknecht[2], Piotr P. Woźniak[3], Vallery Guillou[2], ASTER Team[2a]

[1]University of Gdańsk, Faculty of Oceanography and Geography, Division of Geophysics, Piłsudskiego 46, 81-378 Gdynia, Poland

[2]Aix Marseille Univ., CNRS, IRD, INRAE, CEREGE, Aix-en-Provence, France

[3]University of Gdańsk, Faculty of Oceanography and Geography, Division of Geomorphology and Quaternary Geology, Gdańsk, Poland

*Corresponding author: k.tylmann@ug.edu.pl

[a]Georges Aumaître, Didier Bourlès and Karim Keddadouche

**Non-peer reviewed preprint submitted to EarthArXiv**

**Submitted to *Quaternary Science Reviews* April 30th, 2022**

Highlights:

- New $^{10}$Be ages (n = 25) on and within the ice sheet extent of the Pomeranian Phase (PP)
- Combined analyses of new and recalculated $^{10}$Be ages (n = 86) along the PP ice margin
- Time-transgressive extent of the Scandinavian Ice Sheet (SIS) along the PP ice margin
- Time-slice reconstruction for the southern sector of the last SIS (~20–15 ka)

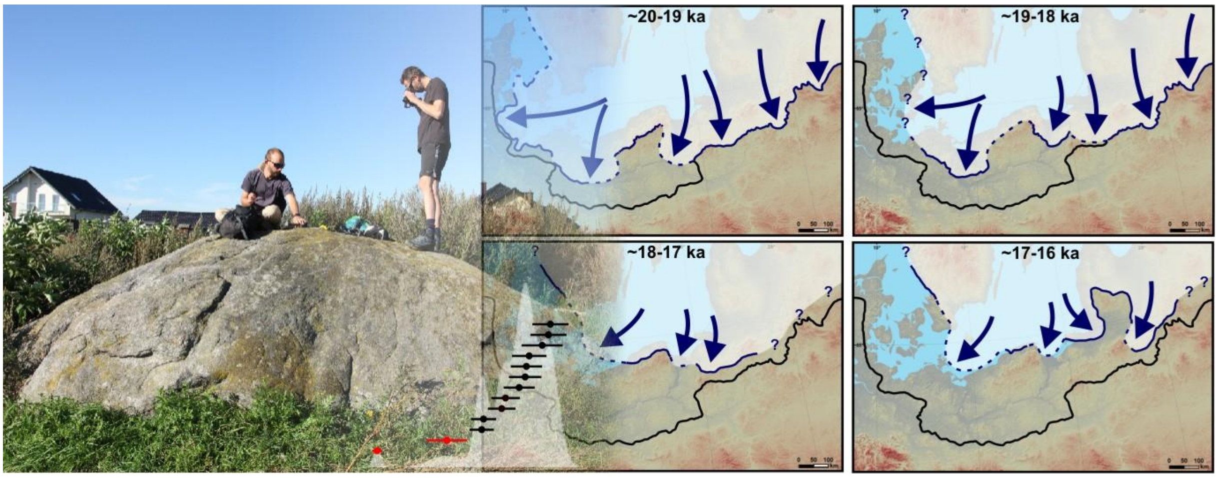

Abstract

We present a new set of 25 $^{10}$Be surface exposure ages of boulders located on the Pomeranian moraines and of erratic boulders located directly upstream of the Pomeranian moraines in northern Poland. Together with recalculated $^{10}$Be surface exposure ages along the Pomeranian Phase ice-marginal belt from Denmark to the west to Lithuania and Belarus to the east, the full data set (n = 86) enabled us to constrain the timing of the ice front standstill and its subsequent retreat. The investigated area consists of geomorphological record along ~2000 km of the ice margin associated with the ice sheet limit correlated so far with the Late Weichselian Pomeranian Phase (Bælthav in Denmark, Baltija in Lithuania and Braslav in Belarus).

We constrained the age of the ice margin position in the area occupied by the Baltic Ice Stream to ~20–19 ka, in the area occupied by the Odra Ice Stream to ~19–18 ka, in the interstream area between the Odra and the Vistula Ice Streams to ~20–19 ka, in the area occupied by the Vistula Ice Stream to ~19–18 ka, in the area occupied by the Mazury Ice Stream to ~18–17 ka, in the area occupied by the Riga Ice Stream to ~17–16 ka, and in the area occupied by the Novgorod Ice Stream to ~16–15 ka. Our best age estimates are based on: (1) a minimum age of the ice margin retreat inferred from new and recalculated $^{10}$Be ages of boulders as well as interpretation of available radiocarbon ages from organic deposits and OSL ages from sediments overlying tills, and (2) a maximum age of the ice margin stillstand and retreat inferred from interpretation of available OSL ages from sandur sediments deposited in front of the ice sheet. The asynchrony of the ice margin positions along the Pomeranian Phase ice-marginal belt shows about 3–5 ka difference between the Bælthav ice margin in Denmark and the Braslav ice margin in Belarus. We propose a new scenario of the Pomeranian Phase ice sheet evolution and a time-slice reconstruction of the last Scandinavian Ice Sheet's southern fringe for the period ~20–15 ka.

Key words: $^{10}$Be surface exposure dating, deglaciation, Pomeranian Phase, Scandinavian Ice Sheet

## 1. Introduction

In the area south of the Baltic Sea, the last Scandinavian Ice Sheet (SIS) formed distinct ice-marginal belts, traditionally ascribed to the three MIS2 (in Europe the Late Weichselian) glacial phases: Brandenburg, Frankfurt and Pomeranian (Woldstedt, 1925, 1935). The ice-marginal landforms of the Brandenburg and the Frankfurt Phases are correlated with the maximum expansion of the last SIS in this region (e.g., Marks, 2012; Tylmann et al., 2019). The Local Last Glacial Maximum was followed by a significant ice-margin standstill which occurred during the Pomeranian Phase (PP). The PP ice sheet limit in northern Poland is morphologically expressed by well-defined terminal moraines, ice-contact sedimentary scarps or proximal edges of proglacial outwash fans/plains (e.g., Galon and Roszkówna, 1961; Roszkówna, 1968; Roman, 1990; Błaszkiewicz, 1998; Kłysz, 2003) which may be correlated with similar landforms in: Denmark (e.g., Houmark-Nielsen, 2007, 2011), northern Germany (e.g., Bremer, 2000; Liedke, 2001), Lithuania (Guobytė, 2004) and Belarus (Karabanov et al., 2004). This association of glacial marginal landforms has a complex origin: in some segments it was formed as a result of recessional standstill of the ice-margin (e.g., Karczewski, 1989; Błaszkiewicz, 1998; 2011), whereas in others the ice margin standstill occurred after the re-advance of ice front (e.g., Müller et al., 1995; Böse, 2005; Guobytė and Satkūnas, 2011). However, based on the geomorphology, the PP ice-marginal belt may be traced across the southern sector of the last SIS as a relatively continuous record of the ice front position correlated with particular phases of deglaciation – Bælthav in Denmark, Pomeranian in Germany and Poland, Baltija in Lithuania, and Braslav in Belarus (cf. Liedtke, 1975; Houmark-Nielsen and Kjær, 2003; Karabanov and Matveyev, 2011; Guobytė and Satkūnas, 2011; Marks, 2015) (Fig. 1). In this regard, the PP ice margin is one of the most prominent ice-marginal features of the Weichselian glaciation in northern Europe (Lüthgens et al., 2011).

It is already well known that during the evolution of the last SIS, particular limits of the ice sheet were time-transgressive (cf. Hughes et al., 2021). The last SIS has never been still along its entire ice margin at a given moment of time, as it is usually presented on traditional glaciomorphological maps, which usually display isochronous ice margin positions by connecting geomorphological features (e.g., Keilhack, 1901; Woldstedt, 1925; Liedtke, 1975). Due to dynamic behavior of particular ice streams and/or diversified response of the ice margin to changing climate, various sectors of the last SIS's southern front advanced and retreated differently over time resulting in a heterogeneous geomorphological record in the glacial landscape, which indeed may reflect asynchronous events. In an effort to capture part of this ice sheet dynamics, numerical dating of ice-marginal landforms could be a base for reconstructions of an asynchronous ice margin that must have continuously existed at a given moment in time (cf. Lüthgens and Böse, 2012).

Surface exposure dating with in-situ produced cosmogenic nuclides is routinely used in developing paleo-ice sheet retreat chronologies (e.g., Corbett et al., 2017; Small et al., 2017; Rinterknecht et al., 2018; Barth et al., 2019; Tylmann et al., 2019; Dulfer et al., 2021). This technique offers direct numerical dating of glacial landforms, using mineral targets in stable erratic boulders resting at the ground surface. The advantage of this method for glacial geochronology is that moraines can be directly dated, instead of their age being constraint by radiocarbon dating of organic material and/or luminescence dating of sandy deposits intercalated between morainic sediments (Ivy-Ochs and Kober, 2008). In-situ cosmogenic nuclides were successfully used in constructing chronologies for MIS 2 paleo-ice sheets (e.g., Marsella et al., 2000; Rinterknecht et al., 2006; Clark et al., 2009). In the case of the last SIS southern periphery, the vastness of the ice-margin studied as well as the streaming behavior of the ice sheet ask for a large chronological dataset to be able to embrace the full picture of the ice margin positions associated with multiple ice streams.

Here, we present a new set of 25 $^{10}$Be surface exposure ages of boulders located on the Pomeranian moraines and of erratic boulders located directly upstream of the Pomeranian moraines in northern Poland. Together with recalculated $^{10}$Be surface exposure ages along the PP ice-marginal belt, the full data set (n = 86) enabled us to constrain the timing of the ice front standstill and its subsequent retreat. We propose a new scenario of the PP ice sheet evolution and a time-slice reconstruction of the last SIS's southern fringe for the period ~20–15 ka. In this study we provide the largest dataset of direct chronology for the southern periphery of the last SIS associated with the PP ice-marginal belt. This chronology makes it possible to understand in details the behavior of an ice stream dominated ice margin in the context of climatic improvement and to understand the response of individual ice streams to local conditions.

## 2. Study area and dating targets

The study area covers the PP ice-marginal belt located south-west, south and south-east of the Baltic basin. It extends from Denmark in the west to Lithuania and Belarus in the east (Fig. 1). The ice sheet limit correlated with the PP is very well traceable in the landscape of northern Europe. It is reconstructed based on the spatial arrangement of ice-marginal landforms, mainly: end moraines and distal outlets of tunnel valleys in Denmark (e.g., Houmark-Nielsen, 2007), end moraines and proximal edges of outwash plains in Germany and Poland (e.g., Liedtke, 2001; Marks, 2012) as well as end moraines and proglacial valleys in Lithuania (e.g., Guobytė and Satkūnas, 2011). The investigated area consists of geomorphological record along ~2000 km of the ice margin associated with the maximum ice sheet limit during the PP. The configuration of this palaeo-ice margin reveals the occurrence of distinct ice lobes, which were shaped by the last SIS palaeo-ice streams operating within the southern periphery of the ice sheet (cf. Punkari, 1995; Boulton et al., 2001). Most of these palaeo-ice streams flowed westwards and southwards from the Baltic basin area. The western segment of the ice margin was shaped by the main Baltic Ice Stream (ice stream $B_1$ according to Punkari's classification) and the southern and eastern segment of the ice margin was shaped by its tributaries: the Odra Ice Stream ($B_2$), the Vistula Ice Stream ($B_3$), the Mazury Ice Stream ($B_4$) and the Riga Ice Stream ($B_5$). The easternmost part of the ice margin was shaped by the Novgorod Ice Stream (F), which flowed from the east European Plain east of the Baltic basin (Fig. 1; Punkari, 1995).

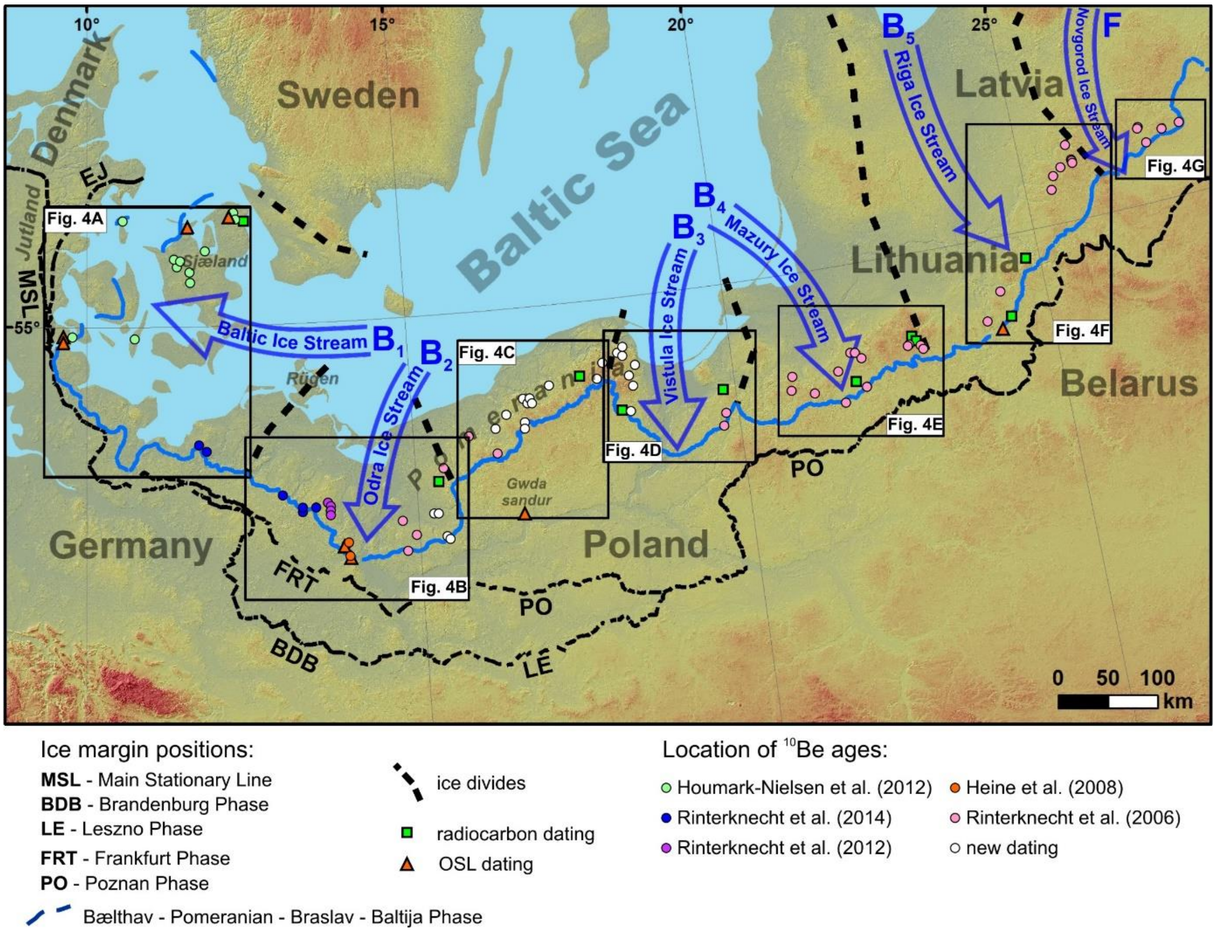


Fig. 1. The study area with reconstructed positions of the Late Weichselian (MIS 2) ice margins. The maximum expansion of the last SIS correlated with the Brandenburg (Leszno) and the Frankfurt (Poznan) Phases are indicated as well as a significant ice-margin standstill, which occurred during the

Pomeranian Phase (light blue lines). Location of $^{10}Be$ dating are marked with circles. Radiocarbon and OSL dating sites significant for the timing of the Pomeranian Phase (PP) ice margin position are marked with squares. Digital elevation model based on SRTM data with a horizontal resolution of 80 m.

$^{10}Be$ dating targets were massive and intact boulders resting on glacial landforms correlated with the PP ice-marginal belt. We choose boulders located exactly on landforms associated with the line indicating maximum extent of the PP ice sheet and those located up to 50 km upstream of the ice sheet flow direction. The full set of $^{10}Be$ ages consists of 61 ages from boulders already dated in previous investigations (Rinterknecht et al., 2006, 2012, 2014; Heine et al., 2008; Houmark-Nielsen et al., 2012) and 25 new ages from boulders from northern Poland (Fig. 1). Sampled boulders are large and stable (embedded into the ground) granitic rocks significantly protruding (at least 0.9 m) above the ground surface (Fig. 2). We analyzed the distribution of all surface exposure ages (n = 86) and in a further step, we analyzed the distributions of ages obtained for boulders located within regions of individual ice streams (Fig. 1). Moreover, we compared the results obtained for boulders located on the moraines indicating the maximum extent of the PP ice sheet, with results obtained for erratic boulders located up to 50 km upstream from the PP ice sheet maximum extent.

Fig. 2. Erratic boulder in northern Poland sampled for $^{10}Be$ dating (sample PM-30).

## 3. Methods

### 3.1. New samples

Samples were taken with a manual jackhammer from the upper surface of 25 boulders (PM samples) of perimeter ranging from 6.6 to 44.0 m and height ranging from 0.9 to 3.8 m (Tab. 1). All boulders are characterized by quartz-rich lithologies as granitoids, granite gneisses and gneisses. In most cases one sample was taken per boulder. On a single occasion we collected two samples from a granitoid boulder with quartz vein located in the area of the

Odra Ice Stream. Sample PM-04A was taken from the granitoid rock, while sample PM-04B was taken from the quartz vein.

Sample preparation was conducted at the Laboratoire National des Nucléides Cosmogéniques in CEREGE, Aix-en-Provence, France. The rock samples were crushed and sieved. The 0.25–1.0 mm fraction was separated with a Frantz magnetic barrier laboratory separator in magnetic and non-magnetic subsamples. Several successive acid attacks of the non-magnetic fractions were performed using a mixture of concentrated hydrochloric acid (HCl) and fluorosilicic acid ($H_2SiF_6$). The purified quartz was decontaminated from meteoric $^{10}$Be by three successive partial dissolutions with concentrated hydrofluoric acid (HF). Decontaminated quartz was dissolved with concentrated HF after adding 100 μL of an home-made $^{9}$Be carrier solution ([$^{9}$Be] = 3025 ± 9 μg/g, Merchel et al., 2008). Beryllium was recovered after two successive separations on ion exchange columns: an anion exchange column (Dowex 1X8) to remove iron and a cation exchange column (Dowex 50WX8) to discard boron and recover Be (Merchel and Herpers, 1999). The eluted Be fractions were precipitated to $Be(OH)_2$ with ammonia and oxidized to BeO. The BeO was mixed with niobium powder to prepare targets and the $^{10}$Be/$^{9}$Be ratios were measured by accelerator mass spectrometry (AMS) at the French National AMS Facility ASTER, Aix-en-Provence (Arnold et al., 2010). The measured $^{10}$Be/$^{9}$Be ratios were normalized relative to the in-house standard STD-11 using an assigned $^{10}$Be/$^{9}$Be ratio of $(1.191 \pm 0.013) \times 10^{-11}$ (Braucher et al., 2015) and a $^{10}$Be half-life of $(1.387 \pm 0.012) \times 10^{-6}$ years (Chmeleff et al., 2010; Korschinek et al., 2010). Analytical 1σ uncertainties include uncertainties in AMS counting statistics, uncertainty in the standard $^{10}$Be/$^{9}$Be, an external AMS error of 0.5% (Arnold et al., 2010), and a chemical blank measurement.

$^{10}$Be ages were calculated using the most recent global production rate (Borchers et al., 2016) and the time dependent scaling scheme for spallation according to Lal (1991) and Stone (2000) (the 'Lm' scaling scheme). We corrected the $^{10}$Be production rate for sample thickness according to an exponential function (Lal, 1991) and assuming an average density of 2.7 g/cm$^3$ for granitoid, granite gneiss and gneiss. The appropriate correction for self-shielding (boulder geometry) was applied when surface of the sampling spot was sloping more than 10°. No correction for the surface erosion of boulders was applied, as we interpret the $^{10}$Be results as minimum age for the ice sheet retreat. All calculations were performed using the online exposure age calculator formerly known as the CRONUS-Earth online exposure age calculator – version 3 (http://hess.ess.washington.edu/math/; accessed: 21.01.2022), which is an updated version of the online calculator described by (Balco et al., 2008). Ages are reported with 1σ uncertainties (including analytical uncertainties and the production rate uncertainty) in Table 1. Where two exposure ages are reported for one boulder (e.g., PM-04, PM-04B) the error-weighted mean age of two samples was calculated.

### 3.2. Recalculated ages

We recalculated $^{10}Be$ ages already published for the PP ice-marginal belt (Rinterknecht et al., 2006, 2012, 2014; Heine et al., 2009; Houmark-Nielsen et al., 2012) following the same procedure of exposure age calculations as described in section 3.1. Recalculated $^{10}Be$ exposure ages are also reported with 1σ uncertainties (including analytical uncertainties and the production rate uncertainty) in Table 1. In the cases where two exposure ages are reported for one boulder (POL-1, POL-1B; POL-4, POL-4B; POL-5, POL-5B; POL-7; POL-7B; LIT-3, LIT-3B) the error-weighted mean age of two samples was calculated.

### 3.3. Timing for the ice margin positions

We estimated the most likely timing for the ice margin positions based on: (1) interpretation of the arithmetic mean age and its uncertainty as the standard deviation of the mean for $^{10}Be$ ages of boulders located within regions of particular ice streams (excluding outliers) as a minimum age of the ice margin retreat in the regions defined by individual ice streams; (2) interpretation of the oldest radiocarbon ages from organic deposits and OSL ages from lacustrine, fluvial and fluvioglacial deposits overlying Upper Weichselian tills associated with particular ice margin positions as a minimum age of the ice margin retreat; (3) interpretation of the OSL ages from sandur sediments deposited in front of the PP ice-marginal belt as a maximum age of the ice margin stillstand and retreat. Therefore, the most likely age of the ice margin positions is proposed as a time interval located between the minimum age of the ice margin retreat and the maximum age of the ice margin stillstand and retreat. Details for the ice margin age estimation within regions of particular ice streams are described in section 5.1.

## 4. Results

### 4.1. Full $^{10}Be$ dataset (n = 86)

$^{10}Be$ ages of boulders scattered along the PP ice-marginal belt range between 3.6 ± 0.5 ka and 84.0 ± 9.1 ka, however the age range between 12.0 ± 1.3 ka and 21.6 ± 2.0 ka fall into a confidence interval arithmetic average ± 1.5 × IQR (interquartile range, which is the range between the third quartile – Q3 and the first quartile – Q1 of the population) (Fig. 3). Variability of the ages falling into this confidence interval (12.7%) slightly exceeds the average analytical uncertainty (10.2%), suggesting that the random uncertainties are dominated by geological uncertainties rather than by analytical ones. The skewness is 0.17 indicating a slightly positively skewed distribution. The arithmetic mean of the 77 exposure ages is 16.7 ± 0.2 ka (standard deviation of the mean) (Fig. 3).

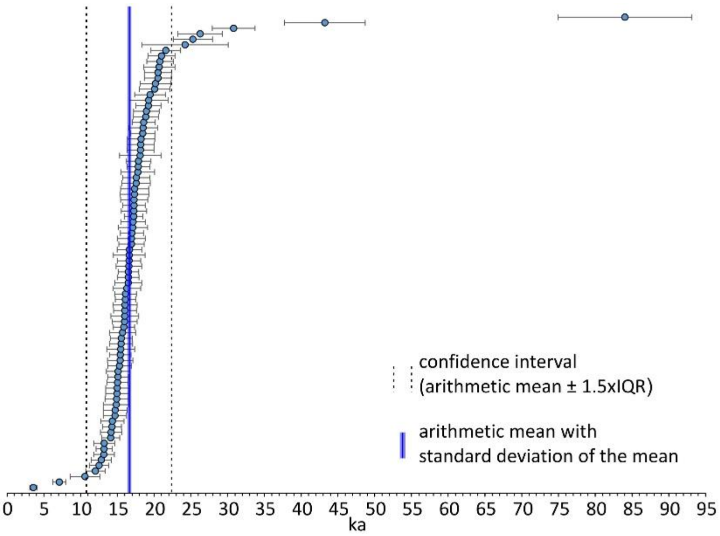


Fig. 3. Distribution of all $^{10}$Be ages (n = 86) analyzed along the PP ice-marginal belt. The dataset consists of 25 new and 61 recalculated ages. The arithmetic mean age and the standard deviation of the mean are calculated for 77 exposure ages belonging to the confidence interval arithmetic mean ± 1.5 × IQR.

## 4.2. Baltic Ice Stream ($B_1$) area

Ages of boulders located in Denmark and northwest Germany, where the main Baltic Ice Stream (BIS) was located, range between 3.6 ± 0.5 ka and 21.0 ± 1.8 ka (Fig. 4A). Distribution of ages (n = 13) is polymodal with the main mode occurring around 18 ka. The reduced chi-squared test indicates that the ages are poorly clustered: $\chi_R^2$ = 55.18. We identify two of the youngest ages (3.6 ± 0.5 ka and 10.6 ± 2.0 ka) as deviating the most from the main mode. They do not fall into a confidence interval arithmetic average ± 1.5 × IQR, and are thus identified as outliers. These “too young” ages may be a result of boulders exposition after deglaciation and/or significant postglacial erosion of sampled surface. After excluding outliers, the remaining 11 ages range between 14.1 ± 1.2 ka and 21.0 ± 1.8 ka and reduced chi-squared test shows a much better cluster: $\chi_R^2$ = 2.76. The variability of the remaining ages is 13.5%, with a $\chi_R^2 > 2$, and the dataset can be described as moderately clustered (Blomdin et al., 2016). The arithmetic mean and the standard deviation of the mean for these 11 surface exposure ages are 17.9 ± 0.7 ka (Fig. 4A).

Reliable $^{10}Be$ ages of boulders located exactly on landforms associated with the line indicating the maximum extent of the PP ice sheet are 18.6 ± 1.6 ka and 17.9 ± 1.6 ka (with an arithmetic mean and a standard deviation of the mean of 18.2 ± 0.4 ka), while $^{10}Be$ ages of boulders located up to 50 km from this line upstream the ice stream pathway range between 14.1 ± 1.2 ka and 21.0 ± 1.8 ka (with an arithmetic mean and a standard deviation of the mean of 17.8 ± 0.9 ka). A t-test shows that for the 95% confidence level we cannot reject the hypothesis that these means are the same (p-value is 0.66). Thus, there is no significance difference between boulder ages on landforms associated with the line indicating maximum extent of the PP ice sheet and those located up to 50 km within the ice stream pathway (Fig. 4A).

### 4.3. Odra Ice Stream ($B_2$) area

In the region where the Odra Ice Stream (OIS) was operating, the highest number of $^{10}Be$ ages were reported among all analyzed regions (n = 24). The ages range between 7.1 ± 0.9 ka and 24.2 ± 5.9 ka, and their distribution is relatively tight with the mode occurring around 16.5 ka (Fig. 4B). However, a reduced chi-squared test shows that these 24 ages are poorly clustered: $\chi_R^2$ = 6.55. The youngest age in the dataset (7.1 ± 0.9 ka) and the oldest (24.2 ± 5.9 ka) were identified as outliers – they lie beyond a confidence interval arithmetic average ± 1.5 × IQR. We invoke similar reasons as for the BIS to explain why one boulder is “too young”.  For the boulder that is “too old”, it most probably contains beryllium inherited from episodes of exposure pre-dating the last deglaciation. After excluding these two outliers, the remaining 22 ages range between 12.0 ± 1.3 ka and 20.1 ± 2.1 ka with a reduced chi-squared test showing a cluster of 1.62. Because $\chi_R^2$ is < 2, and the variability of ages is < 15% (11.1%), we may describe this dataset as well clustered (Blomdin et al., 2016). The arithmetic mean and the standard deviation of the mean are 16.6 ± 0.4 ka (Fig. 4B).

Ten out of twenty-two $^{10}Be$ ages come from boulders located exactly on landforms associated with the line materializing the maximum extent of the PP ice sheet. These ages range between 15.0 ± 1.5 ka and 20.1 ± 2.1 ka , with the arithmetic mean age and the standard deviation of the mean 17.3 ± 0.5 ka. $^{10}Be$ ages of erratic boulders located up to 50 km from this line upstream the ice stream pathway range between 12.0 ± 1.3 ka and 18.9 ± 1.7 ka, with the arithmetic mean age and the standard deviation of the mean 16.0 ± 0.5 ka (Fig. 4B). This slightly younger age of boulders located further to the north may reflect a progressive ice margin retreat. However, a t-test shows that for the 95% confidence level we cannot reject the hypothesis that the mean exposure age of boulders located on landforms associated with the maximum extent of the PP ice sheet and the mean exposure age of boulders located further to the north are the same (p-value is 0.09).

## 4.4. Odra/Vistula interstream area

In the interstream area between the OIS and the Vistula Ice Stream (VIS) $^{10}$Be ages range between 14.7 ± 1.6 ka and 43.2 ± 5.5 ka (n = 13). The distribution is bimodal with the main mode occurring around 16–17 ka (Fig. 4C). The oldest age (43.2 ± 5.5 ka) clearly deviates from the rest of the data set, and it was identified as outlier (beyond the confidence interval mentioned above). After removing this age from the dataset the distribution is unimodal and well clustered as indicated by the reduced chi-squared test: $\chi_R^2$ = 1.51. The ages range between 14.7 ± 1.6 ka and 21.6 ± 2.0 ka with a variability of 12.4%. The arithmetic mean and the standard deviation of the mean for 12 ages are 17.6 ± 0.6 ka (Fig. 4C).

$^{10}$Be ages of four boulders located exactly on landforms associated with the line indicating the maximum extent of the PP ice sheet range between 15.0 ± 1.6 ka and 20.5 ± 1.8 ka (with an arithmetic mean age and a standard deviation of the mean of 17.9 ± 1.1 ka). $^{10}$Be ages of eight boulders located up to 50 km from this line upstream the ice stream pathway range between 14.7 ± 1.6 ka and 21.6 ± 2.0 ka (with an arithmetic mean age and a standard deviation of the mean of 17.4 ± 0.8 ka). This shows that the mean $^{10}$Be ages of boulders located on landforms associated with the line indicating maximum extent of the PP ice sheet and those located up to 50 km from this line towards the interior of the ice sheet are coeval within the range of uncertainty (Fig. 4C). Moreover, a t-test shows that for the 95% confidence level we cannot reject the hypothesis that these means are the same (p-value is 0.73).

## 4.5. Vistula Ice Stream ($B_3$) area

In the region of the VIS we reported ages ranging between 12.8 ± 1.4 ka and 30.8 ± 2.9 ka (n = 11). The distribution is polymodal with a variability of 27% and a $\chi_R^2$ = 6.67 (Fig. 4D). We identify two outliers: 25.3 ± 2.7 ka and 30.8 ± 2.9 ka (ages which lie beyond a confidence interval arithmetic average ± 1.5 × IQR). When these ages are excluded, the remaining nine ages (from 12.8 ± 1.4 ka to 20.7 ± 2.1 ka) show a moderate cluster with variability of 14.6% and a $\chi_R^2$ = 2.35. The arithmetic mean and the standard deviation of the mean for these nine ages are 17.0 ± 0.8 ka (Fig. 4D).

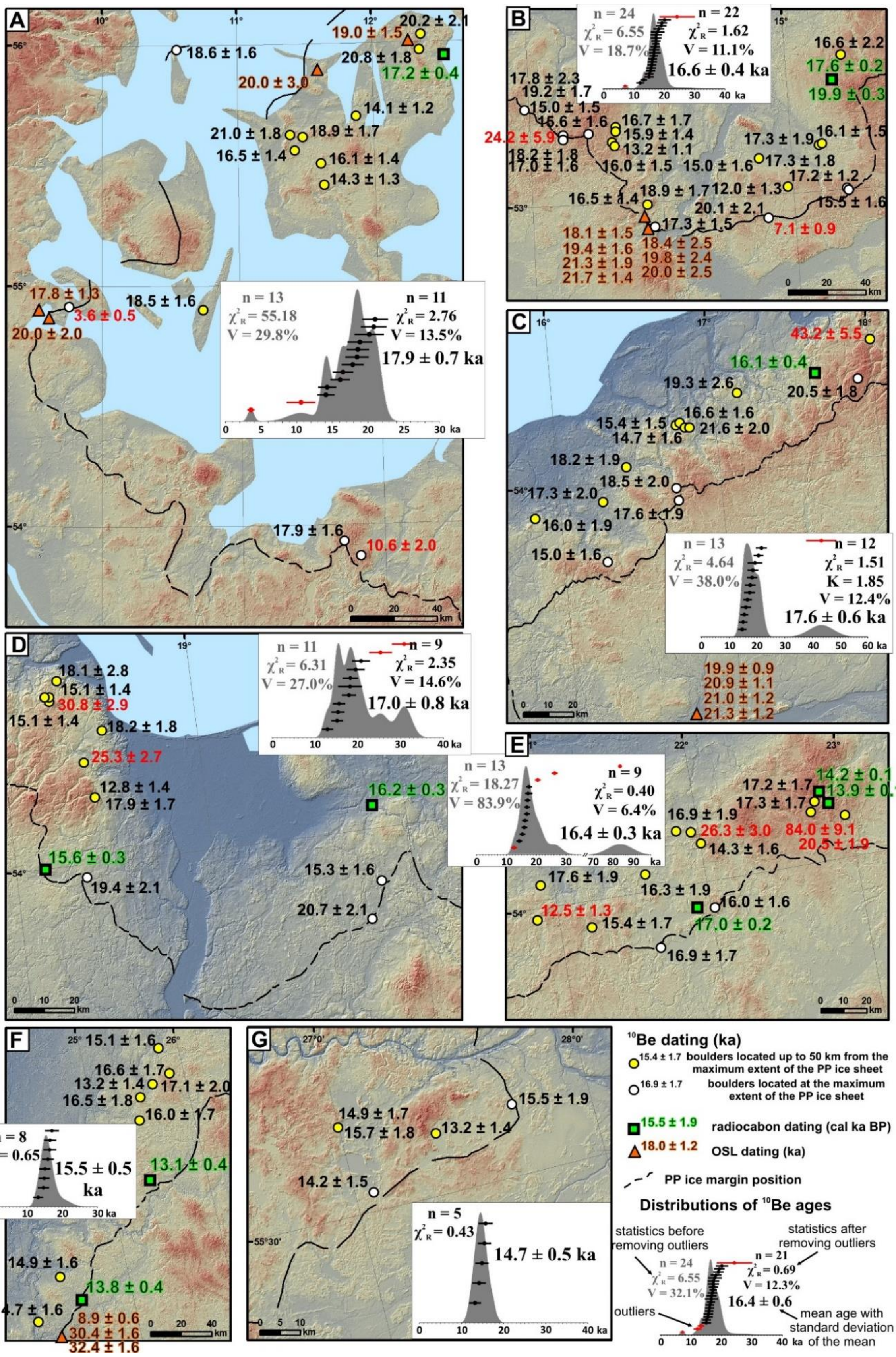

Fig. 4. Location of boulders dated with $^{10}$Be and distributions of $^{10}$Be ages within areas where particular ice streams were operating: (A) Baltic Ice Stream; (B) Odra Ice Stream; (C) Interstream area OIS/VIS; (D) Vistula Ice Stream; (E) Mazury Ice Stream; (F) Riga Ice Stream; (G) Novgorod Ice Stream.

$^{10}$Be ages of three boulders located exactly on landforms associated with the maximum extent of the PP ice sheet are: 15.3 ± 1.6 ka, 19.4 ± 2.1 ka and 20.7 ± 2.1 ka (with an arithmetic mean age and a standard deviation of the mean of 18.5 ± 1.6 ka). $^{10}$Be ages of six boulders located up to 50 km from this line upstream the ice stream pathway range between 12.8 ± 1.4 ka and 18.2 ± 1.8 ka (with an arithmetic mean age and a standard deviation of the mean of 16.3 ± 0.9 ka). The arithmetic means suggest a younger age for boulders located up to 50 km upstream the ice stream pathway (Fig. 4D). However, a t-test shows that for the 95% confidence level we cannot reject the hypothesis that these mean ages are the same (p-value is 0.32).

### 4.6. Mazury Ice Stream ($B_4$) area

Ages of boulders located in northeastern Poland, there where the Mazury Ice Stream (MIS) influenced the ice margin position, range between 12.5 ± 1.3 ka and 84.0 ± 9.1 ka (n = 13). The distribution is bimodal, with the main mode occurring around 16–17 ka. The youngest age (12.5 ± 1.3 ka) and three of the oldest ages (84.0 ± 9.1 ka, 26.3 ± 3.0 ka and 20.5 ± 1.9 ka) do not fall into the confidence interval arithmetic average ± 1.5 × IQR. On this basis, these ages were identified as outliers (Fig. 4E). After removing these ages from the data set the distribution is unimodal and well clustered as indicated by a reduced chi-squared test $\chi_R^2$ of 0.40 and variability of 6.4%. The ages range between 14.3 ± 1.6 ka and 17.6 ± 1.9 ka and the arithmetic mean and the standard deviation of the mean are 16.4 ± 0.3 ka (Fig. 4E).

Two out of nine $^{10}$Be ages come from boulders located exactly on landforms associated with the maximum extent of the PP ice sheet. The ages are 16.0 ± 1.6 ka and 16.9 ± 1.7 ka and the arithmetic mean age and the standard deviation of the mean are 16.5 ± 0.4 ka. $^{10}$Be ages of boulders located up to 50 km from this extent upstream the ice stream pathway range between 14.3 ± 1.6 ka and 17.6 ± 1.9 ka, with an arithmetic mean age and a standard deviation of the mean of 16.4 ± 0.4 ka. This shows that there is no significance difference between ages of boulders on landforms associated with the line indicating maximum extent of the PP ice sheet and those located further upstream of the ice marginal position (Fig. 4E). It is also confirmed by a t-test, which shows that for the 95% confidence level we cannot reject the hypothesis that these mean ages are the same (p-value is 0.98).

### 4.7. Riga Ice Stream ($B_5$) area

In the region occupied by the Riga Ice Stream (RIS), we report $^{10}$Be ages ranging between 13.2 ± 1.2 ka and 17.1 ± 2.0 ka (n = 8). There is no boulders located on landforms associated with the maximum extent, so all the ages come from boulders located up to 50 km from the line indicating the maximum extent of the PP ice sheet upstream the ice stream pathway (Fig. 4F). The distribution is unimodal and well clustered as indicated by a reduced chi-squared test $\chi_R^2$ of 0.65 and an age variability of 8.3%. No outliers were detected and the arithmetic mean age and the standard deviation of the mean are 15.5 ± 0.5 ka.

### 4.8. Novgorod Ice Stream (F) area

In the easternmost area of the Novgorod Ice Stream (NIS) $^{10}$Be ages were reported ranging between 13.2 ± 1.4 ka and 15.7 ± 1.8 ka (n = 5). The distribution is unimodal and well clustered as indicated by a reduced chi-squared test $\chi_R^2$ of 0.43 and an age variability of 6.9%. No outliers were detected and the arithmetic mean age and the standard deviation of the mean are 14.7 ± 0.5 ka (Fig. 4G).

Two out of five $^{10}$Be ages come from boulders located exactly on landforms associated with the maximum extent of the PP ice sheet. These ages are 14.2 ± 1.5 ka and 15.5 ± 1.9 ka with an arithmetic mean age and a standard deviation of the mean of 14.8 ± 0.6 ka. $^{10}$Be ages of boulders located up to 50 km from this extent towards the interior of the ice sheet are 13.2 ± 1.4 ka, 14.9 ± 1.7 ka and 15.7 ± 1.8 ka, with an arithmetic mean age and a standard deviation of the mean of 14.6 ± 0.7 ka. These results show that there is no difference between the ages of boulders located on landforms associated with the line indicating maximum extent of the PP ice sheet and those located further upstream to the north (Fig. 4G). It is also confirmed by a t-test, which demonstrates that for the 95% confidence level we cannot reject the hypothesis that these mean ages are the same (p-value is 0.82).

## 5. Discussion

### 5.1. Ages of the ice margin positions

Our results show that the most likely ages of ice margin positions correlated so far with the Pomeranian Phase of the Late Weichselian (Bælthav in Denmark, Baltija in Lithuania and Braslav in Belarus) vary between ~20 ka and ~15 ka along the southern front of the last SIS from the BIS region to the west to the sector of NIS to the east (Fig. 5). We constrained the age of the ice margin position in the area occupied by the BIS to ~20–19 ka. This is based on the $^{10}$Be minimum age of the ice margin retreat (17.9 ± 0.7 ka) as well as OSL ages of the Late Glacial lacustrine mud and fluvial sand overlying the Mid Danish and Young Baltic tills in Sjælland and southeast Jutland ranging between 20.0 ± 3.0 ka and 17.8 ± 1.3 ka (Fig. 4A; Houmark-Nielsen and Kjær, 2003). The oldest radiocarbon age of the Late

Glacial lacustrine deposits overlying the Young Baltic tills within ice sheet extent of the Bælthav Phase is 17.2 ± 0.4 cal ka BP obtained from bone found at the Nivå section in northeastern Sjælland (Tab. 2). If the age of the bone is equivalent to the age of deposits, it could suggest that the ice sheet retreat from the Bælthav ice marginal belt occurred earlier. However, age of the Bælthav ice margin position constrained to ~20–19 ka is older than the timing of the ice re-advances after the recession from the Main Stationary Line (MSL) in Denmark. The latter was estimated based on lithostratigraphic and chronostratigraphic investigations of the Upper Weichselian sediments at 19–18 ka and 18–17 ka for the two Young Baltic advances which deposited the East Jylland and Bælthav ice-marginal formations (Houmark-Nielsen and Kjær, 2003; Krohn et al., 2009; Larsen et al., 2009). Stroeven et al. (2016) followed Houmark-Nielsen and Kjær (2003) when correlating the East Jylland with the Frankfurt and Poznań ice-marginal formations, and the Bælthav with the Pomeranian ice-marginal formation in Germany and Poland, and constrained the isochronous retreat of the last SIS along the Bælthav ice-marginal belt to 18–17 ka. In the reconstruction of the last Eurasian ice sheet of Hughes et al. (2016) for the time-slice 19 ka the minimum ice extents are located within the area of the Bælthav ice-marginal belt. Furthermore, a thermomechanical ice sheet model for the retreat of the Eurasian ice sheet complex after 23 ka (Patton et al., 2017) shows that, in the optimal deglaciation scenario, the Bælthav ice-marginal formation lies mostly between isochrones of 21 ka and 18 ka, which is supported by our age estimation in this sector of the ice sheet (Fig. 6A).

For the segment of the PP ice-marginal belt under the influence of the OIS (Figs. 1, 4B), we constrained the most likely age of the ice margin position to ~19–18 ka (Fig. 5). The minimum age of the ice margin retreat calculated with all $^{10}$Be ages in the region is 16.4 ± 0.4 ka. However, the mean $^{10}$Be age of boulders located exactly on the maximum extent of the PP ice sheet is 17.3 ± 0.5 ka. Moreover, the oldest calibrated radiocarbon ages of organic deposits overlying a till, which may also indicate minimum age of deglaciation in this area, are 19.9 ± 0.3 and 17.6 ± 0.2 cal ka BP (Tab. 2; Fig. 4B). Based on OSL dating of sandur deposits, Lüthgens et al. (2011) constrained the age of the Pomeranian ice margin position in Germany between 20.1 ± 1.6 ka and 19.4 ± 2.4 ka (Fig. 5). This gives quite a wide time estimate based on various geochronological methods (from 20.1 to 16.4 ka). The reasons could be that: (1) $^{10}$Be surface exposure dating enables to constrain the minimum age of deglaciation, because boulders exposition to cosmic rays may occur during ice margin retreat or later, i.e. during dead-ice melting and/or landforms stabilisation (cf. Houmark-Nielsen et al., 2012; Lüthgens et al., 2011); it follows that the ice margin stabilisation at the PP ice-marginal belt may predate surface exposure age of boulders; (2) radiocarbon dating of the oldest lacustrine/peat deposits of the lake basins located to the north of the PP ice-marginal belt also constrain the minimum age of deglaciation, as lake sediments started to accumulate as soon as dead ice melted (e.g., Błaszkiewicz, 2011); however, in case of reworking of material for radiocarbon dating, ages could be “too old” and could be even older than the actual timing of the ice margin stillstand and retreat; (3) OSL dating of glacial deposits such as sandar, enables to constrain the time of proglacial outwash deposition, which may occur before or during ice margin stabilisation as well as during ice margin retreat. Therefore, various dating techniques may constrain timing of various processes occurring during ice margin stillstand and deglaciation, which may be reflected in a wide range of obtained ages.

The maximum extent of the last SIS in eastern Germany and western Poland occurred during the Brandenburg (Leszno) Phase, not earlier than ~25–24 ka as indicated by calibrated radiocarbon ages of organic deposits underlying the Upper Weichselian till (e.g., Ehlers et al., 2011; Marks, 2012; Tylmann et al., 2019). OSL dating of sand underlying the upper most till at Rügen suggests, that the ice advance to the Late Weichselian maximum must have occurred between 25 ka and 21 ka (Kenzler et al., 2015, 2017; Pisarska-Jamroży et al., 2018). The retreat of the ice sheet from the maximum limit in eastern Germany occurred not later than 22.1 ± 0.9 ka as indicted by surface exposure ages from Brandenburg (Heine et al., 2009) recalculated with a global $^{10}$Be production rate (Borchers et al., 2016). The Pomeranian ice margin position must thus post-date the phase of the maximum ice extent and also the phase of recessional ice margin stillstand (Frankfurt Phase). This is clearly inferred from morphostratigraphic relations between particular ice marginal belts (Fig. 6A and B). We propose an age of the PP ice marginal position within the OIS region constrained to ~19–18 ka as the best age estimate. This corresponds to the minimum age of the Pomeranian ice sheet retreat from its maximum extent at 17.3 ± 0.5 ka. It overlaps with the age range of sandur deposits 21.7–17.0 ka and partly agrees with the oldest radiocarbon ages of post glacial deposits. The radiocarbon ages (19.9 ± 0.3 and 17.6 ± 0.2 cal ka BP) may be however overestimated as bulk carbonate material (gyttja) was dated (Fig. 5; Tab. 2), opening the possibility that an age overestimation was caused by a freshwater reservoir effect related to water enriched in ancient dissolved calcium carbonates, the so called “hard water effect” (e.g., Philippsen, 2013).

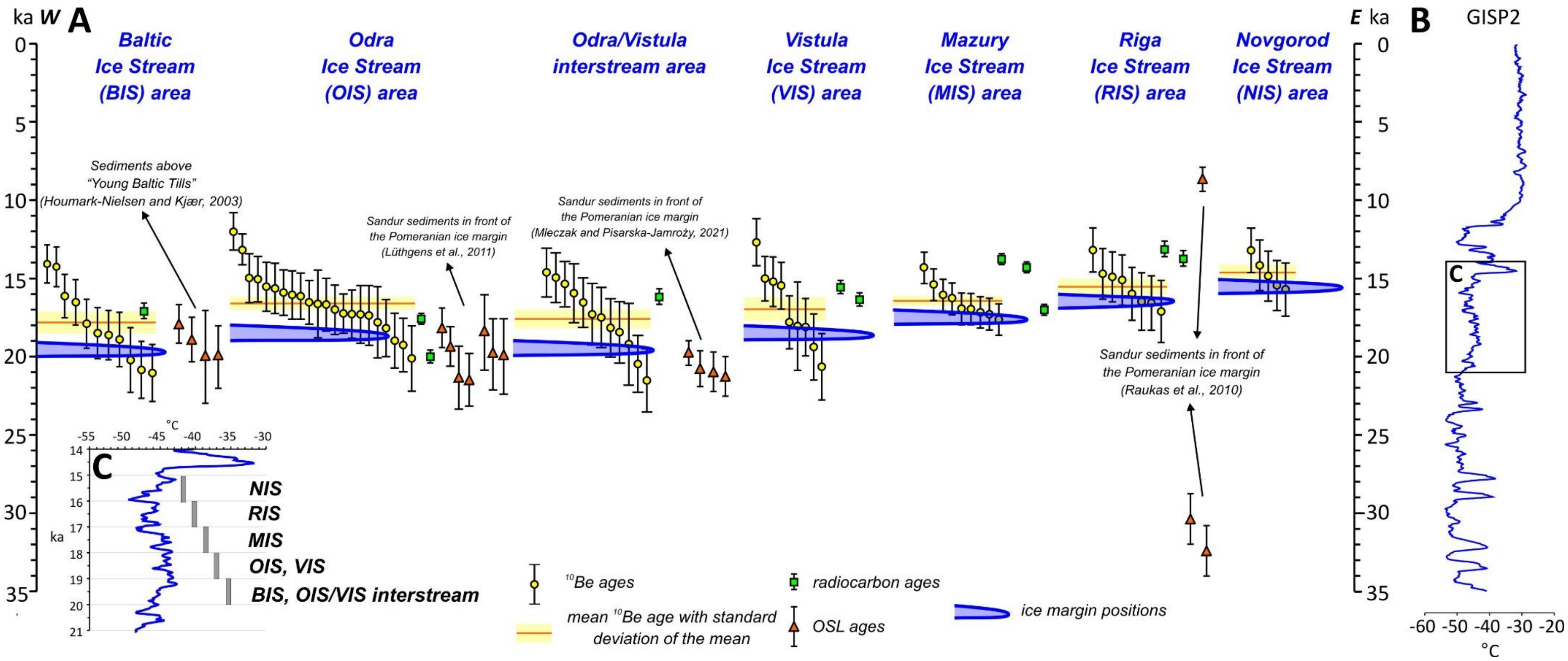


Fig. 5. (A) Timing of the ice margin positions along the PP ice-marginal belt. $^{10}$Be ages used in mean surface exposure age calculations are shown against the radiocarbon and OSL ages significant for the timing of the PP ice margin positions. (B) Variability of palaeotemperatures inferred from the GISP2 ice core record (Alley, 2004) is shown for the period 0–35 ka. (C) Most probable ages of ice margin positions estimated in this study (grey bars) are shown against the paleotemperature variability between 21 ka and 14 ka.

In the central part of Pomerania in Poland, between the areas occupied by the OIS and the VIS (Figs. 1 and 4C) we constrained the most likely age of the Pomeranian ice margin position to ~20–19 ka. The minimum age for the ice margin retreat calculated based on $^{10}Be$ ages is 17.6 ± 0.6 ka, and it is comparable with the BIS mean $^{10}Be$ age obtained in the region (17.9 ± 0.7 ka). The oldest calibrated radiocarbon age of organic deposits formed after the ice margin retreated from the PP ice-marginal belt is 16.1 ± 0.4 cal ka BP (Tab. 2; Fig. 4C). However, the average age of outwash deposits from the distal part of the Gwda sandur deposited in front of the PP ice-marginal belt is 20.8 ± 1.1 ka (Mleczak and Pisarska-Jamroży, 2021). This indicates that around 22–20 ka the ice margin in this region was already situated to the north of the Frankfurt (Poznań) ice-marginal belt. The deposition of the Gwda sandur might have started during a progressive recession of the ice sheet after the Frankfurt (Poznań) Phase and before the ice margin stillstand along the PP ice-marginal belt. Taking into account the minimum age of deglaciation inferred from $^{10}Be$ ages and radiocarbon ages of lake deposits, as well as ages of the Gwda sandur deposits the best age estimate for the ice margin position in central Pomerania is ~20–19 ka.

We constrained the most likely age of the Pomeranian ice margin position to ~19–18 ka in the VIS region, based on the mean $^{10}Be$ age of all samples 17.0 ± 0.7 ka, the mean $^{10}Be$ age of boulders located exactly on landforms associated with the line indicating maximum extent of the PP ice sheet 18.5 ± 1.6 ka (n = 3), and the oldest calibrated radiocarbon ages of organic deposits formed after the ice margin retreated 16.2 ± 0.3 and 15.6 ± 0.3 cal ka BP (Tab. 2; Fig. 4D). Taking into account the possible age of the local LGM in central and eastern Poland 22–18 ka (Tylmann et al., 2019), the age of the Pomeranian ice margin position in the VIS area constrained to ~19–18 ka is very likely (Fig. 6A and B). Similarly, our age constraints of ~18–17 ka in the MIS region, ~17–16 ka in the RIS region and ~16–15 ka in the NIS region are robust when we compare them with the most likely age of the last SIS maximum extent there (Fig. 6B). We inferred these constraints mainly from the mean $^{10}Be$ age of boulders and erratics supported by the oldest radiocarbon ages of sediments formed after the ice margin retreated (Figs. 4E-G). OSL ages of sandur deposits in front of the PP ice-marginal belt in the RIS region do not reflect the actual timing of the ice margin standstill (Raukas et al., 2010). Two ages (32.4 ± 1.6 and 30.4 ± 1.6 ka) are clearly too old (possibly due to incomplete bleaching of sediment grains) and one age (8.9 ± 0.6 ka) is much too young for the Late Pleistocene deposits (Fig. 4F). One radiocarbon age from western Belarus (Zimenkov, 1989) provides an age for the last SIS maximum extent in the eastern part of the study area at ~22.5 cal ka BP (Tylmann et al., 2019). Surface exposure $^{10}Be$ ages of boulders and erratics located on and upstream the last SIS maximum extent in the Valday Heights (northwestern Russia, north east of the NIS region) constrained the timing (minimum age) of the local LGM to 20.1 ± 0.4 ka (Rinterknecht et al., 2018). The ages of the ice margin positions along the PP ice-marginal belt in the easternmost sectors of the study area are constrained to ~17–16 ka (RIS) and ~16–15 ka (NIS) which is significantly younger than the local LGM.

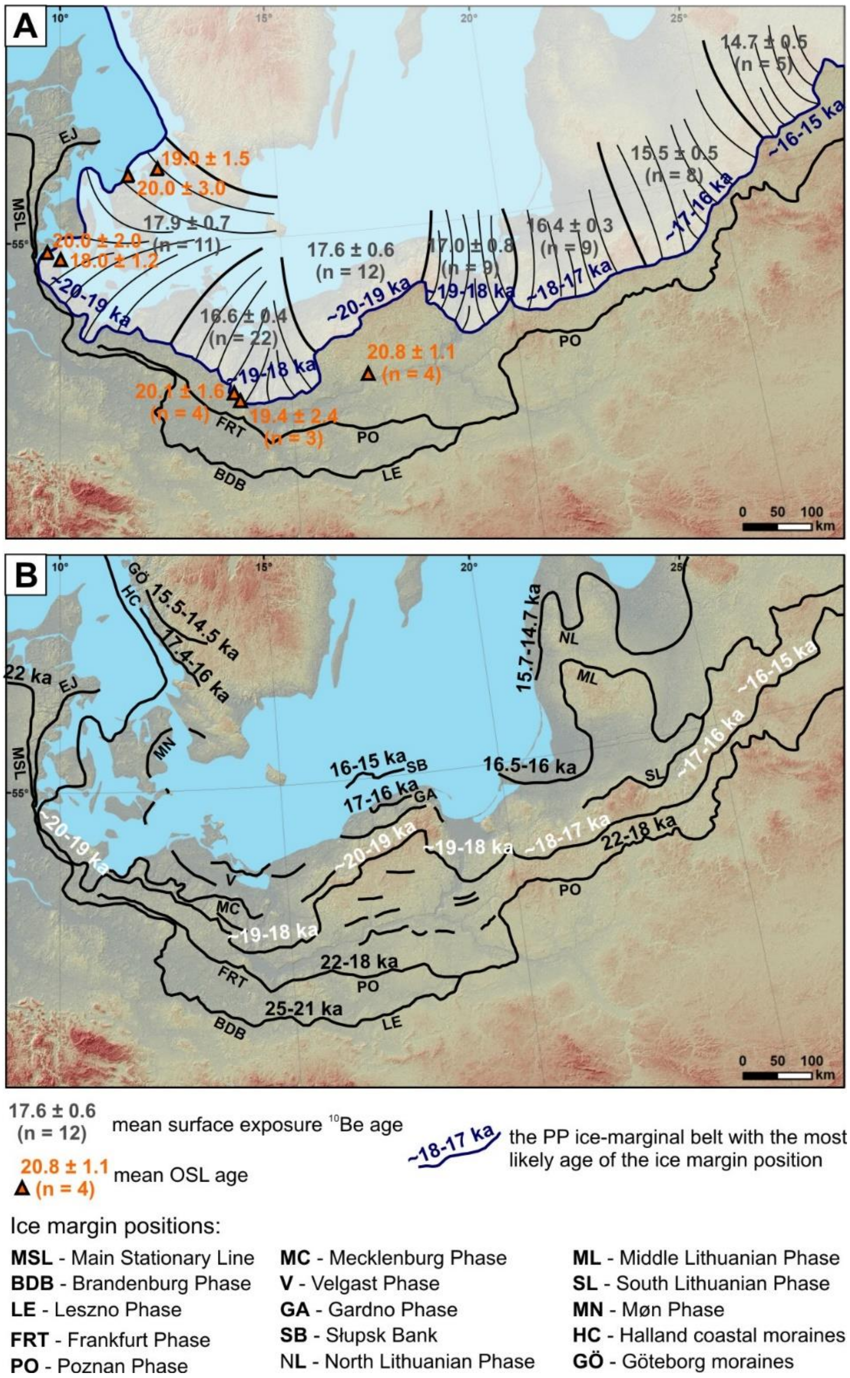


Fig. 6. Extents of the last SIS during Late Weichselian glacial phases and their ages. (A) Ages of ice margin positions along the PP ice-marginal belt. The best age estimates of ice margin positions within particular regions was constrained based on the mean $^{10}$Be age of boulders and erratics, available OSL

ages and the oldest radiocarbon ages (see Fig. 5). (B) Ages of the ice marginal positions along the PP ice-marginal belt proposed in this study against the most likely ages for other Late Weichselian ice sheet limits known from the literature: Brandenburg (Leszno) and Frankfurt (Poznań) Phase (Tylmann et al., 2019); Main Stationary Line (Houmark-Nielsen and Kjær, 2003; Larsen et al., 2009); Halland coastal and Göteborg moraines (Stroeven et al., 2016); Gardno and Słupsk Bank Phase (Tylmann and Uścinowicz, in press); Middle Lithuanian and South Lithuanian Phases (Kalm, 2006; Lasberg and Kalm, 2013).

### 5.2. New scenario for ice margin positions and time-slice reconstruction (~20–15 ka)

We propose a new scenario of the ice margin dynamics along the PP ice-marginal belt in the European Lowland (Fig. 7). The maximum extent of the last SIS in the area south of the Baltic basin occurred ~25–22 ka in the western sector of the ice sheet (Denmark, Germany, western Poland) during the Brandenburg (Leszno) Phase and ~22–18 ka in the eastern sector (central and eastern Poland, Lithuania, Belarus) during the Frankfurt (Poznań) Phase (Tylmann et al., 2019). After the local LGM the ice sheet started to retreat. However, during this period of general deglaciation ice margin stillstands and/or local re-advances also occurred. The re-advances were most likely triggered by ice streams operating within the southern periphery of the last SIS. Most of these ice streams were located along the Baltic basin and were active not only during the ice sheet advance phase, but also during deglaciation (Punkari, 1995, 1997). The existence of several ice streams along the southern front of the last SIS was probably the main factor controlling the time-transgressive development of ice margins and diachronous formation of particular ice-marginal formations (e.g., Marks, 2002).

After recession of the ice margin from the Main Stationary Line in Denmark an ice re-advance occurred resulting in the formation of the Bælthav ice-marginal belt about 20–19 ka. Similar timing of the ice margin position was also estimated for the PP ice-marginal belt in central Pomerania in Poland. Age of the last SIS maximum extent in the eastern part of the study area may be roughly constrained to ~19–18 ka (e.g., Wysota et al., 2009; Marks, 2012; Larsen et al., 2016; Hughes et al., 2021), and in Germany, the age of the Frankfurt ice-marginal formation could be interpreted to ~20–18 ka (e.g., Litt, 2007; Marks, 2015). Thus, around 20–19 ka ago the ice margin was located along the Bælthav ice-marginal belt in Denmark and the Pomeranian ice-marginal formation in northwestern Germany. The ice sheet formed conspicuous ice lobes which terminated at the Frankfurt ice-marginal formation in northeastern Germany. In northwestern Poland, the eastern part of the ice lobe joined the Pomeranian ice-marginal belt of central Pomerania. Further to the east, the ice margin formed another ice lobe which probably linked the central Pomeranian ice margin with the maximum extent of the last SIS to the east (Fig. 7A). About 19–18 ka ago, the OIS and the VIS formed two conspicuous ice lobes in Poland (the Odra Ice Lobe and the Vistula Ice Lobe). The ice margin between the ice lobes was probably located in northern part of the Pomerania (interlobate zone). Location of the ice margin to the west of the OIS is difficult to reconstruct, while to the east of the VIS the ice margin most likely went eastwards where it merged with the maximum extent of the last SIS (Fig. 7B).

About 18–17 ka ago, the ice margin was located at the Halland coastal moraine complex as it could be inferred from the recent dating of those moraines to 17.4–16.0 ka (Fig. 6B; Stroeven et al., 2016). The ice margin ran from the Halland coastal moraines to the southeast, across the Baltic basin, and was located along one of the recessional marginal belts in Pomerania in Poland. Further to the east, a small ice lobe could have linked this belt with the PP ice-marginal formation in the MIS region (Fig. 7C). The ice margin to the east of the MIS region at ~18–17 ka is more difficult to reconstruct, and its position remains rather unknown. Around 17–16 ka ago the ice margin was probably still located along the Halland coastal moraines, it ran across the Baltic basin forming an extensive ice lobe, which terminated at the northern edge of Rügen and met the Gardno ice-marginal belt in the present coastal area of Poland (Fig. 7D). The existence of the ice lobe in the southwestern Baltic basin at that time was reconstructed based on possible extension of the Gardno ice-marginal belt at the seafloor along the present Polish coastline (cf. Uścinowicz, 1999), and on correlation of the Gardno moraines with the north Rügen moraines (Tylmann, Uscinowicz in press). To the east of the Gardno ice-marginal belt, the ice margin probably formed a small lobe, which linked this marginal formation with the western segment of the Middle Lithuanian moraines, dated usually at 16.5–16.0 ka (Fig. 6B), based on calibrated radiocarbon ages and OSL ages (Kalm, 2006; Lasberg, Kalm, 2013). In the eastern sector of the study area a narrow ice lobe probably developed, linking the Middle Lithuanian moraines with the segment of the PP ice-marginal belt in the RIS region. The western flank of the ice lobe terminated at the Middle Lithuanian moraines, while the eastern flank terminated at the PP ice-marginal belt (Fig. 7D).

The last time-slice that we reconstructed is the most likely configuration if the ice margin at ~16–15 ka (Fig. 7E). In the western sector, the ice margin retreated from the Halland coastal moraines to the line of the Göteborg moraines, which were recently dated at 15.5–14.5 ka (Fig. 6B; Lundqvist and Wohlfarth, 2001; Stroeven et al., 2016). To the southeast from the Göteborg moraines, the ice margin ran across the Baltic to the Słupsk Bank Phase ice-marginal belt reconstructed based on relicts of ice marginal landforms at the Baltic seafloor (e.g., Uścinowicz, 1999) and recently dated at ~15.2 ka (Uścinowicz et al., 2019) and

15.5 ± 0.5 ka (Tylmann and Uścinowicz, in press). From the Słupsk Bank the ice margin most likely went northeast to the North Lithuanian ice-marginal belt, recently dated at 15.7–14.7 ka (Fig. 6B) based on calibrated radiocarbon ages and OSL ages (Kalm, 2006; Lasberg and Kalm, 2013). In the easternmost part of the study area the ice margin was linked by a narrow ice lobe to the segment of the PP ice-marginal belt formed by the NIS (Fig. 7E).

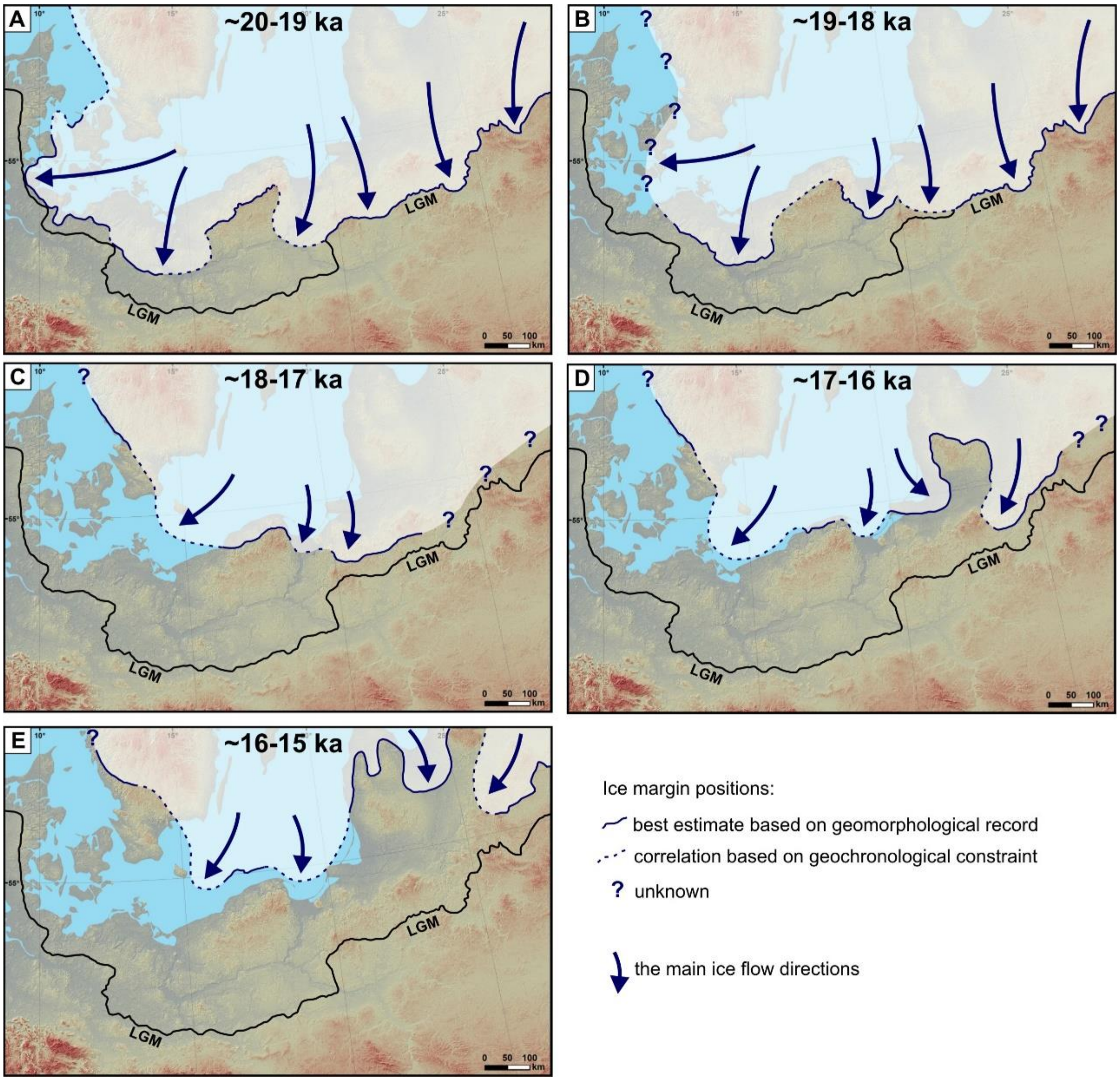


Fig. 7. Time-slice reconstruction of the southern SIS for the period ~20–15 ka. (A) Ice margin position around 20–19 ka. (B) Ice margin position around 19–18 ka. (C) Ice margin position around 18–17 ka. (D) Ice margin position around 17–16 ka. (E) Ice margin position around 16–15 ka.

## 5.3. Asynchrony and asymmetry of the southern SIS

The asynchrony of the ice margin positions along the PP ice-marginal belt shows about 3–5 ka difference between the Bælthav ice margin in Denmark and the Braslav ice margin in Belarus (Fig. 6A). The general trend is that the ice margin positions are getting younger eastward, except in central Pomerania in Poland, where the age of the ice margin position is similar to the age of the Bælthav ice margin in Denmark. To the west and to the east of central Pomerania in the OIS and VIS regions, the ice margin positions are about 1 ka younger. The documented time-transgressive character of the PP ice-marginal belt was most likely caused by spatial and temporal variability of the last SIS dynamics triggered by activation and deactivation of particular ice streams (e.g., Stokes and Clark, 1999; Boulton et al, 2001). Dynamics of various segments of the ice margin and particular ice streams could be related to climatic conditions occurring along the southern periphery of the last SIS or to local topographic and/or glaciologic parameters influencing the ice margin fluctuation (e.g. facilitating ice streaming). Larsen et al. (2016) suggested that causes of the time-transgressive glacial maxima positions of the last SIS may be explained by glaciodynamic responses to geographically variable physical boundary conditions. Over a large area such as the southern periphery of the last SIS these variable conditions could be: (1) migration of the main ice divide during ice sheet build-up, (2) distance to ice-inception center, (3) topography and type of subglacial bed or (4) thermal regime at the ice/bed interface and ice flow mechanisms. Some of these factors are climatically driven (e.g. windward ice sheet growth), whereas others are purely local (e.g. topography and type of subglacial bed). Diversified timing of the ice margin stillstands along the PP ice-marginal belt is to some extent a continuation of the time-transgressive glacial maxima positions (Larsen et al., 2016; Hughes et al., 2021) as the PP ice-marginal landforms were formed during the general recession of the last SIS from its maximum extent. Another factor could be related to the wide distance range to the ice-inception center, which for the eastern segment of the ice margin was longer than for the western sector, possibly delaying the ice accumulation impulse towards the ice margin in the eastern sector. Moreover, the western segment of the ice margin retreated largely within the Baltic basin, where extensive ice-dammed lakes were formed in front of the ice sheet (e.g., Uścinowicz, 1999; Andrén, 2012). This could have triggered a more dynamic behavior of the ice margin (earlier and faster advances and retreats due to the water influence) in comparison to the mainly land-based (and potentially also frozen to bed) eastern sectors (Larsen et al., 2016).

The time-slice reconstruction shows that the southern periphery of the last SIS during the period 20–15 ka is characterized by a clear asymmetry: the western sector retreated earlier and much further to the north from the line of the maximum extent than the eastern sector (Fig. 7). Moreover, in the western sector of the southern SIS many more ice margin positions are recorded in the landscape compare to the eastern sector (Fig. 6B). During the time-slice

20–19 ka in the western sector of the study area, the ice margin was located almost at the same place as the maximum extent of the last SIS or up to ~30 km away from it, while in the eastern sector the ice sheet was at its maximum extent (Fig. 7A). During the time-slice 16–15 ka in the western sector of the study area, the ice margin was already located as far as ~230–360 km from the maximum extent of the last SIS, while in the eastern periphery of the study area the ice margin was only ~60–85 km from the maximum extent (Fig. 7E). This highlights that for the period ~20–15 ka the western sector of the ice margin was much more dynamic than the eastern sector. The difference could be a response of the ice sheet to the maritime climate influences from the west and/or a response to the presence of proglacial lakes in front of the ice margin as well as the dominance of warm ice in the western sector of the southern SIS.

## 6. Conclusions

Our study provides the largest dataset for a direct chronology of the southern periphery of the last SIS associated with the PP ice-marginal belt. A new set of 25 $^{10}$Be surface exposure ages of boulders located on the Pomeranian moraines and of erratic boulders located directly upstream of the Pomeranian moraines in northern Poland. Together with recalculated $^{10}$Be surface exposure ages along the PP ice-marginal belt in the European Lowland we document a clear asynchrony of the ice margin positions with about 3–5 ka difference between the Bælthav ice margin in Denmark and the Braslav ice margin in Belarus. Our best age estimates constrain the timing of the ice margin positions in the area occupied by: (1) the Baltic Ice Stream at ~20–19 ka, (2) the Odra Ice Stream at ~19–18 ka, (3) the interstream zone between the Odra and the Vistula Ice Streams at ~20–19 ka, (4) the Vistula Ice Stream at ~19–18 ka, (5) the Mazury Ice Stream at ~18–17 ka, (6) the Riga Ice Stream at ~17–16 ka, and (7) the Novgorod Ice Stream at ~16–15 ka. The time-transgressive character of the PP ice-marginal belt was most likely caused by spatial and temporal variability of the last SIS dynamics triggered by activation and deactivation of particular ice streams.

The time-slice reconstruction of the last SIS's southern fringe inferred from the age constraint of the ice margin positions reveals a new scenario of the PP ice sheet evolution over the ~20–15 ka period. The southern periphery of the last SIS during this period is characterized by a clear asymmetry: the western sector retreated earlier and much further to the north from the line of the PP maximum extent than the eastern sector. The more dynamic behavior of the western sector compare to the eastern sector of the ice margin might result from the maritime climatic influences from the wests and/or the abundance of water in front of the ice sheet as well as the dominance of warm ice in the western sector of the southern SIS.

Acknowledgements: We are very grateful to the Regional Directorates of Environmental Protection local communes offices for permissions for sampling large erratics protected by law.

Funding: This work was supported by the National Science Center in Poland [grant no. 2014/15/D/ST10/04113 to Karol Tylmann]. The ASTER AMS national facility (CEREGE, Aix en Provence) is supported by the INSU/CNRS, the ANR through the “Projets thematiques d'excellence” program for the “Equipements d'excellence” ASTER-CEREGE action and IRD

References

Alley, R.B., 2004. GISP2 Ice Core Temperature and Accumulation Data. IGBP PAGES/World Data Center for Paleoclimatology Data Contribution Series #2004-013. NOAA/NGDC Paleoclimatology Program, Boulder CO, USA.

Andrén, T., 2012. Baltic Sea Basin, Since the Latest Deglaciation. In: Bengtsson L., Herschy R.W., Fairbridge R.W. (Eds) Encyclopedia of Lakes and Reservoirs. Encyclopedia of Earth Sciences Series. Springer, Dordrecht.

Arnold, M., Merchel, S., Bourlés, D.L., Braucher, R., Benedetti, L., Finkel, R.C., Aumaître, G., Gottdang, A., Klein, M., 2010. The French accelerator mass spectrometry facility ASTER: Improved performance and developments. Nuclear Instruments and Methods in Physics Research B 268, 1954–1959.

Balco, G., Stone, J.O., Lifton, N.A., Dunai, T.J., 2008. A complete and easily accessible means of calculating surface exposure ages or erosion rates from $^{10}$Be and $^{26}$Al measurements. Quaternary Geochronology 3, 174–195.

Barth, A.M., Marcott, S.A., Licciardi, J.M., Shakun, J.D., 2019. Deglacial Thinning of the Laurentide Ice Sheet in the Adirondack Mountains, New York, USA, Revealed by $^{36}$Cl Exposure Dating. Paleoceanography and Paleoclimatology 34, 946–953.

Blomdin, R., Stroeven, A.P., Harbor, J.M., Lifton, N.A., Heyman, J., Gribenski, N., Petrakov, Caffee, M.W., Ivanov, M.N., Hättestrand, C., Rogozhina, I., Usubaliev, R., 2016. Evaluating the timing of former glacier expansions in the Tian Shan: A key step towards robust spatial correlations. Quaternary Science Reviews 153, 78–96.

Błaszkiewicz, M., 1998. The Wierzyca Valley, its genesis and development in late Pleistocene and early Holocene (in Polish with English summary). Dokument. Geogr., 10.

Błaszkiewicz, M., 2011. Timing of the final disappearance of permafrost in the central European Lowland, as reconstructed from the evolution of lakes in N Poland. Geological Quarterly 55, 361–374.

Borchers, B., Marrero, S., Balco, G., Caffee, M., Goehring, B., Lifton, N., Nishiizumi, K., Philips, F., Schaefer, J., Stone, J., 2016. Geological calibration of spallation production rates in the CRONUS-Earth project. Quaternary Geochronology 31, 188–198.

Boulton, G.S., Dongelmans, P., Punkari, M., Broadgate, M., 2001. Palaeoglaciology of an ice sheet through a glacial cycle: the European ice sheet through the Weichselian. Quaternary Science Reviews 20, 591–625.

Böse, M., 2005. The Last Glaciation and Geomorphology. In: E.A. Koster (Ed.) The Physical geography of Western Europe. Oxford University Press, 61–74.

Braucher, R., Guillou, V., Bourlès, D. L., Arnold, M., Aumaître, G., Keddadouche, K., Nottoli, E., 2015. Preparation of ASTER in-house $^{10}$Be/$^{9}$Be standard solutions. Nuclear Instruments and Methods in Physics Research B 361, 335–340.

Bremer, F., 2000. Geologische Übersichtskarte von Mecklenburg-Vorpommern 1:500.000. LUNG M-V, Güstrow.

Chmeleff, J., von Blanckenburg, F., Kossert, K., Jakob, D., 2010. Determination of the $^{10}$Be half-life by multicollector ICP-MS and liquid scintillation counting. Nuclear Instruments and

Methods in Physics Research Section B: Beam Interactions with Materials and Atoms 268, 192–199.

Clark, J., McCabe, C.M., Schnabel, C., Clark, P.U., McCarron, Freedman, S.P.H.T., Maden, C., Xu, S., 2009. Cosmogenic $^{10}$Be chronology of the last deglaciation of western Ireland, and implications for sensitivity of the Irish Ice Sheet to climate change. Geological Society of America Bulletin 121, 3–16.

Corbett, L.B., Bierman, P.R., Larsen, P., Stone, B.D., Caffee, M.W., 2017. Cosmogenic nuclide age estimate for Laurentide Ice Sheet recession from the terminal moraine, New Jersey, USA, and constraints on Latest Pleistocene ice sheet behavior. Quaternary Research 87, 482–498.

Czernik, J., 2009. Radiocarbon dating of Late Glacial sediments of Lake Miłkowskie by accelerator mass spectrometry. Acta Palaeobotanica 49, 337–352,

Dulfer, H., Margold, M., Engel, Z., Braucher, R., ASTER Team, 2021. Using $^{10}$Be dating to determine when the Cordilleran Ice Sheet stopped flowing over the Canadian Rocky Mountains. Quaternary Research 102, 222–233.

Ehlers, J., Grube, A., Stephan, H.-J., Wansa, S., 2011. Pleistocene Glaciations of North Germany–New Results. In: Ehlers, J., Gibbard, P.L., Hughes P.D. (Eds.) Quaternary Glaciations - Extent and Chronology: A Closer Look. Elsevier Amsterdam, 149–162.

Galon, R, Roszkówna, L., 1961. Extents of the Scandinavian glaciations and of their recession stages on the Territory of Poland in the light of an analysis of the marginal forms of inland ice. Prz. Geogr. 33, 347–361.

Gałka, M., Sznel, M., 2013. Late Glacial and Early Holocene development of lakes in northeastern Poland in view of plant macrofossil analyses. Quaternary International 292, 124–135.

Guobytė, R., 2004. A brief outline of the Quaternary of Lithuania and the history of its investigation. In: Ehlers, J., Gibbard P.L., (Eds.) Quaternary Glaciations – Extent and Chronology, Part I: Europe. Elsevier, Amsterdam, 245–250.

Guobytė, R., Satkūnas, J., 2011. Pleistocene Glaciations in Lithuania. In: Ehlers J., Gibbard, P.L., Hughes, P.D. (Eds.) Quaternary Glaciations – Extent and Chronology: A Closer Look. Developments in Quaternary Science, 15. Elsevier, Amsterdam, 231–246.

Heine, K., Reuther, A.U., Thieke, H.U., Schulz, R., Schlaak, N., Kubik, P.W., 2009. Timing of Weichselian ice marginal positions in Brandenburg (northeastern Germany) using cosmogenic in situ $^{10}$Be. Zeitschrift für Geomorphologie NF 53, 433–454.

Houmark-Nielsen, M., 2007. Extent and age of Middle and Late Pleistocene glaciations and periglacial episodes in southern Jylland, Denmark. Bulletin of the Geological Society of Denmark 55, 9–35.

Houmark-Nielsen, M., 2011. Pleistocene Glaciations in Denmark: A closer Look at chronology, Ice Dynamics and Landforms. In: Ehlers, J., Gibbard, P.L. Hughes, P.D. (Eds.) Quaternary Glaciations – Extent and Chronology: A Closer Look. Developments in Quaternary Science, 15. Elsevier, Amsterdam, 47–58.

Houmark-Nielsen, M., Kjær, K.H., 2003. Southwest Scandinavia, 40–15 kyr BP: palaeogeography and environmental change. Journal of Quaternary Science 18, 769–786.

Hughes, A.L.C., Winsborrow, M.C.M., Greenwood, S.L., 2021. European Ice Sheet Complex evolution during the Last Glacial Maximum (29–19 ka). In: Palacios, D., Hughes, P.D., García-Ruiz, J.M., Andrés, N. (Eds.) European Glacial Landscapes. Maximum Extent of Glaciations. Elsevier, 361–372.

Ivy-Ochs, S., Kober, F., 2008. Surface exposure dating with cosmogenic nuclides. Eiszeitalter und Gegenwart Quaternary Science Journal 57, 179–209.

Kalm, V., 2006. Pleistocene chronostratigraphy in Estonia, southeastern sector of the Scandinavian glaciation. Quaternary Science Reviews 25, 960–975.

Karabanov, A.K., Matveyev, A.V., 2011. The Pleistocene Glaciations in Belarus. In: Ehlers, J., Gibbard, P.L., Hughes, P.D. (Eds.) Quaternary Glaciations – Extent and Chronology: A Closer Look. Developments in Quaternary Science, 15. Elsevier, Amsterdam, 29–35.

Karabanov, A.K., Matveyev, A.V., Pavlovskaya, I.E., 2004. The main glacial limits in Belarus. In: Ehlers, J., Gibbard, P.L. (Eds.) Quaternary Glaciations: Extent and Chronology. Elsevier B.V., Amsterdam, 15–18.

Karczewski, A., 1989. Morphogenesis of the ice-marginal zone of the Pomeranian Phase in the area of the Parsęta Ice Lobe during Vistulian (Middle Pomerania). University of Adam Mickiewicz Press, Poznań, Geography Series 44 (in Polish).

Keilhack, K ., 1901. Geologisch-Morfologische Überschichstkarte der Provinz Pommern. 1:500 000. Königl. Preuss. Geol. Landesanst. u. Bergakad., Berlin.

Kenzler, M., Tsukamoto, S., Meng, S., Thiel, C., Frechen, M., Hüneke, H., 2015. Luminescence dating of Weichselian interstadial sediments from the German Baltic Sea coast. Quaternary Geochronology 30, 215–256.

Kenzler, M., Tsukamoto, S., Meng, S., Frechen, M., Hüneke, H., 2017. New age constraints from the SW Baltic Sea area – implications for Scandinavian Ice Sheet dynamics and palaeoenvironmental conditions during MIS 3 and early MIS 2. Boreas 46, 34–52.

Kłysz, P., 2003. Maximum limits of the Baltic ice-sheet during the Pomeranian Phase in the Drawskie Lakeland. Quaestiones Geographicae 22, 29–42.

Korschinek, G., Bergmaier, A., Faestermann, T., Gerstmann, U.C., Knie, K., Rugel, G., Wallner, A., Dillmann, I., Dollinger, G., von Gostomski, C.L., 2010. A new value for the half-life of $^{10}$Be by Heavy-Ion Elastic Recoil Detection and liquid scintillation counting. Nuclear Instruments and Methods in Physics Research Section B: Beam Interactions with Materials and Atoms 268, 187–191.

Krohn, C.F., Larsen, N.K., Kronborg, C., Nielsen, O.B., Knudsen, K.L. 2009. Litho- and chronostratigraphy of the Late Weichselian in Vendsyssel, northern Denmark with special emphasis on tunnel-valley infill in relation to a receding ice margin. Boreas 38, 811–833.

Lagerlund, E., Houmark-Nielsen, M., 1993. Timing and pattern of the last deglaciation in the Kattegat region, southwest Scandinavia. Boreas 22, 337–347.

Lauterbach, S., Brauer, A., Andersen, N., Danielopol, D.L., Dulski, P., Hüls, M., Milecka, K., Namiotko, T., Plessen, B., Von Grafenstein U., DecLakes Participants, 2011. Multi-proxy evidence for early to mid-Holocene environmental and climatic changes in northeastern Poland. Boreas 40, 57–72.

Lal, D., 1991. Cosmic ray labeling of erosion surfaces: In situ nuclide production rates and erosion models. Earth Planetary Science Letters 104, 424–439.

Larsen, E., Fredin, O., Lyså, A., Amantov, A., Fjeldskaar, W., Ottesen, D., 2016. Causes of time-transgressive glacial maxima positions of the last Scandinavian Ice Sheet. Norwegian Journal of Geology 96, 159–170.

Larsen, N.K., Knudsen, K.L., Krohn, C.F., Ronborg, C., Murray, A.S., Nielsen, O.B., 2009. Late Quaternary ice sheet, lake and sea history of southwest Scandinavia – a synthesis. Boreas 38, 732–761.

Lasberg, K., Kalm, V., 2013. Chronology of Late Weichselian glaciation in the western part of the East European Plain. Boreas 42, 995–1007.

Liedtke, H., 1975. Die Nordischen Vereisungen in Mitteleuropa. Forschungen zur deutschen Landeskunde 204, Bonn–Bad Godesberg.

Liedtke, H., 2001. Das nordöstliche Brandenburg während der Weichseleiszeit. In: S. Bussemer (Ed.), Das Erbe der Eiszeit, Beier & Beran, Langenweissbach, 119–133.

Litt, T., Behre, K.E., Meyer, K.D., Stephan, H.J., Wansa, S., 2007. Stratigraphische Begriffe für das Quartär des norddeutschen Vereisungsgebietes, E&G Quaternary Science Journal 56, 7–65.

Lundqvist, J., Wohlfarth, B., 2001. Timing and east-west correlation of south Swedish ice marginal lines during the Late Weichselian. Quaternary Science Reviews 20, 1127–1148.

Lüthgens, C., Böse, M., 2012. From morphostratigraphy to geochronology – on the dating of ice marginal positions. Quaternary Science Reviews 44, 26–36.

Lüthgens, C., Böse, M., Preusser, F., 2011. Age of the Pomeranian ice-marginal position in northeastern Germany determined by Optically Stimulated Luminescence (OSL) dating of glaciofluvial sediments. Boreas 40, 598–615.

Marks, L., 2002. Last Glacial Maximum in Poland. Quaternary Science Reviews 21, 103–110.

Marks, L., 2012. Timing of the Late Vistulian (Weichselian) glacial phases in Poland. Quaternary Science Reviews 44, 81–88.

Marks, L., 2015. Last deglaciation of northern Continental Europe. Cuadernos Investigacion Geografica 41, 279–297.

Marsella, K.A., Bierman, P.R., Davis, P.T., Caffee, M.W., 2000. Cosmogenic Be-10 and Al-26 ages for the Last Glacial Maximum, eastern Baffin Island, Arctic Canada. Geological Society of America Bulletin 112, 1296–1312.

Merchel, S., Arnold M., Aumaître, G., Benedetti, L., Bourlès, D.L., Braucher, R., Alfimov, V., Freeman, S.P.H.T., Steier, P., Wallner, A., 2008. Towards more precise $^{10}$Be and $^{36}$Cl data from measurements at the 10−14 level: Influence of sample preparation. Nuclear Instruments and Methods in Physics Research Section B: Beam Interactions with Materials and Atoms 266, 4921–4926.

Merchel, S., Herpers, U., 1999. An update on radiochemical separation techniques for the determination of long-lived radionuclides via accelerator mass spectrometry, Radiochimica Acta 84, 215–220.

Mleczak, M., Pisarska-Jamroży, G., 2021. A record of deglaciation-related shifting of the proximal zone of a sandur – a case study from the Gwda sandur, NW Poland (MIS 2). Journal of Palaeogeography 10, doi.org/10.1186/s42501-021-00089-x.

Müller, U., Rühberg, N., Krienke, H.-D., 1995. The Pleistocene sequence in Mecklenburg-Vorpommern. In: Ehlers, J., Kozarski, S., Gibbard, P.L. (Eds.) Glacial deposits in North-East Europe. Rotterdam, Balkema A.A. Publishers, 501–514.

Neustadt, M., 1971. About the lower boundary of the Holocene. In: Neustadt, M. (Ed.): Palynology of the Holocene, Institut Geografii Akademii Nauk SSSR (Academy of Sciences of the USSR Publishers), Moscow, 7– 13.

Niewiarowski, W., 2003. Pleni- and Late Vistulian glacial lakes, their sediments and landforms: a case study from the young glacial landscape of Northern Poland. Prace Geograficzne 128, 133–142.

Patton, H., Hubbard, A., Andreassen, K., Auriac, A., Whitehouse, P.L., Stroeven, A.P., Shackleton, C., Winsborrow, M., Heyman, J., Hall, A.M., 2017. Deglaciation of the Eurasian ice sheet complex. Quaternary Science Reviews 169, 148–172.

Philippsen, B., 2013. The freshwater reservoir effect in radiocarbon dating. Heritage Science 1, 1–24.

Pisarska-Jamroży, M., Belzyt, S., Börner, A., Hoffmann, G., Hüneke, H., Kenzler, M., Obst, K., Rother, H., van Loon, A.J., 2018. Evidence from seismites for glacio-isostatically induced crustal faulting in front of an advancing land-ice mass (Rügen Island, SW Baltic Sea). Tectonophysics 745, 338–348.

Punkari, M., 1995. Function of the ice streams in the Scandinavian ice sheet: analyses of glacial geological data from southwestern Finland. Transactions of the Royal Society of Edinburgh: Earth Sciences 85, 283–302.

Punkari, M., 1997. Glacial and glaciofluvial deposits in the interlobate areas of the Scandinavian ice sheet. Quaternary Science Reviews 16, 741–753.

Raukas, A., Stankowski, W., Zelčs, V., Šinkunas, P., 2010. Chronology of the last deglaciation in the southeastern Baltic region on the basis of recent OSL dates. Geochronometria 36, 47–54.

Reimer, P.J., Austin, W.E.N., Bard, E., Bayliss, A., Blackwell, P.G., Bronk Ramsey. C,, Butzin, M., Cheng, H., Edwards, R.L., Friedrich, M., Grootes, P.M., Guilderson, T.P., Hajdas, I., Heaton, T.J., Hogg, A.G., Hughen, K.A., Kromer, B., Manning, S.W., Muscheler, R., Palmer, J.G., Pearson, C., van der Plicht, J., Reimer, R.W., Richards, D.A., Scott, E.M., Southon, J.R., Turney, C.S.M., Wacker, L., Adolphi, F., Büntgen, U., Capano, M., Fahrni, S.M., Fogtmann-Schulz, A., Friedrich, R., Köhler, P., Kudsk, S., Miyake, F., Olsen, J., Reinig, F., Sakamoto, M., Sookdeo, A., Talam, S., 2020. The IntCal20 northern hemisphere radiocarbon age calibration curve (0–55 cal ka BP). Radiocarbon 62, 725–757.

Rinterknecht, V.R., Börner, A., Bourlès, D., Braucher, R., 2014. Cosmogenic $^{10}$Be dating of ice sheet marginal belts in Mecklenburg-Vorpommern, Western Pomerania (northeast Germany). Quaternary Geochronology 19, 42–51.

Rinterknecht, V., Braucher, R., Böse, M., Bourlès, D., Mercier, J.L., 2012. Late Quaternary ice sheet extents in northeastern Germany inferred from surface exposure dating. Quaternary Science Reviews 44, 89–95.

Rinterknecht, V.R., Clark, P.U.M., Raisbeck, G.M, Yiou, F., Bitinas, A., Brook, E.J., Marks, L., Zelcs, V., Lunkka, J.P., Pavlovskaya, I.E., Piotrowski, J.A., Raukas, A., 2006. The last deglaciation of the southeastern sector of the Scandinavian Ice Sheet. Science 311, 1449–1452.

Rinterknecht, V., Hang, T., Gorlach, A., Kohv M., Kalla, K., Kalm, V., Subetto, D., Bourlès, D., Léanni, L., Guillou, V., ASTER Team, 2018. The Last Glacial Maximum extent of the Scandinavian Ice Sheet in the Valday Heights, western Russia: Evidence from cosmogenic surface exposure dating using $^{10}$Be. Quaternary Science Reviews 200, 106–113.

Roman, M., 1990. Zlodowacenie Wisły w rejonie Bramki w zachodniej części Pojezierza Mazurskiego. Kwartalnik Geologiczny 34, 325–338.

Roszkówna, L., 1968. Recesja ostatniego lądolodu z terenu Polski. In: Galon, R. (Ed.) Ostatnie zlodowacenie skandynawskie w Polsce. Pr. Geogr. Inst. Geogr. PAN 74, 65–100.

Serebryanny, L.R., 1978. The Dynamics of Continental Ice Sheet and Glacio-eustasy in the Late Quaternary Time, Nauka, Moscow.

Small, D., Benetti, S., Dove, D., Ballantyne, C.K., Fabel, D., Clark, C.D., Gheorghiu, D.M., Newall, J., Xu, S., 2017. Cosmogenic exposure age constraints on deglaciation and flow behavior of a marine-based ice stream in western Scotland, 21–16 ka. Quaternary Science Reviews 167, 30–46.

Stokes, C.R., Clark, C.D., 1999. Geomorphological criteria for identifying Pleistocene ice streams. Annals of Glaciology 28, 67–74.

Stone, J., 2000. Air pressure and cosmogenic isotope production. Journal of Geophysical Research 105, 23753–23760.

Stroeven, A.P., Hättestrand, C., Kleman, J., Heyman, J., Fabel, D., Fredin, O., Goodfellow, B.W., Harbor, J.M., Jansen, J.D., Olsen, L., Caffee, M.W., Fink, D., Lundqvist, J., Rosqvist, G.C., Strömberg, B., Jansson, K.N., 2016. Deglaciation of Fennoscandia. Quaternary Science Reviews 147, 91–121.

Tylmann, K., Rinterknecht, V.R., Woźniak, P.P., Bourlès, D., Schimmelpfennig, I., Guillou, V., ASTER Team, 2019. The Local Last Glacial Maximum of the southern Scandinavian Ice Sheet front: Cosmogenic nuclide dating of erratics in northern Poland. Quaternary Science Reviews 219, 36–46.

Tylmann, K., Uścinowicz, Sz., Timing of the last deglaciation phases in the southern Baltic area inferred from Bayesian age modeling. Quaternary Science Reviews, in press.

Uścinowicz, Sz., 1999. Southern Baltic area during the last deglaciation. Geological Quarterly 43, 137–148.

Uścinowicz, Sz., Adamiec, G., Bluszcz, A., Jegliński, W., Jurys, L., Miotk-Szpiganowicz, G., Moska, P., Pączek, U., Piotrowska, P., Poręba, G., Przezdziecki, P., Uścinowicz, G., 2019. Chronology of the last ice sheet decay on the southern Baltic area based on dating of glaciofluvial and ice-dammed lake deposits. Geological Quarterly 63, 192–207.

Woldstedt, P., 1925. Die großen Endmoränenzüge Norddeutschlands. Zeitschrift der Deutschen Geologischen Gesellschaft 77, 172–184.

Woldstedt, P., 1935. Geologisch-morphologische Übersichtskarte des norddeutschen Vereisungsgebietes. Preußische Geologische Landesanstalt, Berlin.

Wysota, W., Molewski, P., Sokołowski, R.J., 2009. Record of Vistula ice lobe advance in the Late Weichselian glacial sequence in north-central Poland. Quaternary International 207, 26–41.

Zimenkov, O., 1989. Age of the maximum extent of the Poozerian Glaciation in Belarus. New data about Cenozoic geology of Belarus and adjacent areas. In: Matveyev, A. (Ed.), Nauka I Tekhnika, Minsk, Belarus (in Russian), 30–44.

Table 1. Surface exposure $^{10}$Be ages of erratic boulders located on the PP ice-marginal belt. The list consists of 25 new $^{10}$Be ages (PM samples) and 61 ages recalculated from the original data of Heine et al. (2009), Houmark-Nielsen et al. (2012), Rinterknecht et al. (2006; 2012; 2014). All $^{10}$Be exposure ages are calculated with ‘Lm’ time-dependent scaling scheme for spallation according to Lal (1991) and Stone (2000) and the global production rate according to Borchers et al. (2016).

| **Sample ID** | **Latitude N DD** | **Longitude E DD** | **Elevation (m a.s.l.)** | **Sample thickness (cm)** | **Shielding factor[1]** | **Quartz (g)** | **[$^{10}$Be] ($10^4$ at $g^{-1}$)** | **Age (ka)** |
|---|---|---|---|---|---|---|---|---|
| **Baltic Ice Stream area** | | | | | | | | **17.9 ± 0.7** |
| SJAE-0705 | 55.4068 | 11.6268 | 45 | 2.0 | 1.0000 | n.a. | 6.29 ± 0.30 | 14.3 ± 1.3 |
| SJAE-0706 | 55.9640 | 12.3500 | 20 | 2.5 | 1.0000 | n.a. | 8.89 ± 0.39 | 20.8 ± 1.8 |
| SJAE-0707 | 55.4981 | 11.6044 | 35 | 3.0 | 1.0000 | n.a. | 6.96 ± 0.29 | 16.1 ± 1.4 |
| SJAE-0708 | 55.5544 | 11.4090 | 50 | 3.0 | 1.0000 | n.a. | 7.25 ± 0.32 | 16.5 ± 1.4 |
| SJAE-0709 | 55.6182 | 11.3859 | 35 | 3.5 | 1.0000 | n.a. | 9.04 ± 0.38 | 21.0 ± 1.8 |
| SJAE-0710 | 55.6067 | 11.4725 | 45 | 4.0 | 1.0000 | n.a. | 8.18 ± 0.43 | 18.9 ± 1.7 |
| SJAE-0711 | 55.6931 | 11.8703 | 15 | 4.0 | 1.0000 | n.a. | 5.92 ± 0.26 | 14.1 ± 1.2 |
| SJAE-0712 | 56.0281 | 12.3609 | 40 | 2.0 | 1.0000 | n.a. | 8.85 ± 0.61 | 20.2 ± 2.1 |
| FYN-0801 | 54.8972 | 10.7333 | 4 | 2.0 | 1.0000 | n.a. | 7.76 ± 0.36 | 18.5 ± 1.6 |
| *JYL-0803* | *54.9117* | *9.7618* | *50* | *2.0* | *1.0000* | *n.a.* | *1.59 ± 0.19* | *3.6 ± 0.5** |
| JYL-0808 | 55.9785 | 10.5589 | 30 | 2.0 | 1.0000 | n.a. | 8.08 ± 0.31 | 18.6 ± 1.6 |
| *MVP-15* | *53.8658* | *11.8275* | *115* | *1.8* | *1.0000* | *31.4463* | *4.99 ± 0.87* | *10.6 ± 2.0** |
| MVP-16 | 53.9272 | 11.7106 | 82 | 1.1 | 1.0000 | 32.4840 | 8.17 ± 0.36 | 17.9 ± 1.6 |
| **Odra Ice Stream area** | | | | | | | | **16.6 ± 0.4** |
| MVP-1 | 53.3272 | 13.4503 | 113 | 1.3 | 1.0000 | 34.2125 | 7.33 ± 0.51 | 15.6 ± 1.6 |
| *MVP-2* | *53.3244* | *13.2572* | *94* | *2.3* | *1.0000* | *5.6888* | *11.05 ± 2.52* | *24.2 ± 5.9** |
| MVP-3 | 53.3042 | 13.2523 | 76 | 0.8 | 1.0000 | 13.1803 | 8.23 ± 0.54 | 18.2 ± 1.8 |
| MVP-18 | 53.4494 | 12.9647 | 90 | 3.7 | 1.0000 | 30.5874 | 8.00 ± 0.82 | 17.8 ± 2.3 |
| MVP-19 | 53.4503 | 12.9647 | 99 | 1.0 | 1.0000 | 31.1386 | 6.98 ± 0.42 | 15.0 ± 1.5 |
| MVP-20 | 53.4503 | 12.9647 | 100 | 2.3 | 1.0000 | 25.3464 | 8.84 ± 0.41 | 19.2 ± 1.7 |
| BER-97-01 | 53.3491 | 13.6505 | 82 | 2.0 | 0.9999 | 11.3085 | 7.53 ± 0.51 | 16.7 ± 1.7 |

| | | | | | | | | |
|---|---|---|---|---|---|---|---|---|
| BER-97-02 | 53.3250 | 13.6642 | 80 | 2.0 | 0.9884 | 25.6505 | 7.08 ± 0.36 | 15.9 ± 1.4 |
| BER-97-03 | 53.2814 | 13.6364 | 91 | 2.0 | 0.9999 | 14.7713 | 6.01 ± 0.22 | 13.2 ± 1.1 |
| BER-97-04 | 53.2629 | 13.6493 | 80 | 2.0 | 1.0000 | 17.2591 | 7.23 ± 0.43 | 16.0 ± 1.5 |
| BER-97-05 | 53.2640 | 13.6480 | 60 | 2.0 | 1.0000 | 18.9498 | 7.49 ± 0.40 | 17.0 ± 1.6 |
| PO-05-01 | 52.8800 | 13.9200 | 80 | 5.0 | 1.0000 | n.a. | 8.30 ± 0.39 | 17.3 ± 1.5 |
| PO-05-02 | 52.9800 | 13.8700 | 73 | 3.0 | 1.0000 | n.a. | 9.20 ± 0.49 | 18.9 ± 1.7 |
| PO-05-03 | 52.9800 | 13.8600 | 75 | 5.0 | 1.0000 | n.a. | 7.90 ± 0.29 | 16.5 ± 1.4 |
| *POM-12* | *52.8856* | *14.7914* | *80* | *1.0* | *1.0000* | *70.063* | *3.09 ± 0.30* | *7.1 ± 0.9** |
| POM-13 | 52.8856 | 14.7914 | 80 | 1.0 | 1.0000 | 70.190 | 8.73 ± 0.62 | 20.1 ± 2.1 |
| POM-16 | 53.1669 | 14.7358 | 96 | 1.5 | 1.0000 | 60.244 | 6.60 ± 0.47 | 15.0 ± 1.6 |
| POM-17 | 53.0175 | 14.9544 | 60 | 1.5 | 1.0000 | 70.023 | 5.10 ± 0.40 | 12.0 ± 1.3 |
| POM-18 | 53.6133 | 15.4369 | 102 | 1.0 | 1.0000 | 69.931 | 7.42 ± 0.78 | 16.6 ± 2.2 |
| PM-01 | 53.2181 | 16.2552 | 62 | 3.0 | 0.9976 | 24.27 | 7.05 ± 0.36 | 16.1 ± 1.5 |
| PM-02 | 53.2089 | 15.2299 | 60 | 1.6 | 1.0000 | 19.10 | 7.65 ± 0.57 | 17.3 ± 1.8 |
| PM-03 | 53.2091 | 15.2299 | 60 | 1.2 | 1.0000 | 19.65 | 7.70 ± 0.61 | 17.3 ± 1.9 |
| PM-04A | 52.9963 | 15.4031 | 96 | 1.9 | 1.0000 | 24.75 | 8.63 ± 0.58 | 18.8 ± 1.9 |
| PM-04B | 52.9963 | 15.4031 | 96 | 2.0 | 1.0000 | 19.06 | 7.21 ± 0.56 | 15.8 ± 1.7 |
| PM-04^ | | | | | | | | 17.2 ± 1.2 |
| PM-05 | 52.9784 | 15.4213 | 95 | 2.5 | 1.0000 | 19.87 | 7.05 ± 0.47 | 15.5 ± 1.6 |
| **Odra/Vistula interstream area** | | | | | | | | **17.6 ± 0.6** |
| POM-21 | 53.7117 | 16.2553 | 133 | 2.0 | 1.0000 | 70.14 | 6.860 ± 0.510 | 15.0 ± 1.6 |
| POM-22 | 53.8906 | 15.8381 | 110 | 1.5 | 1.0000 | 23.49 | 7.190 ± 0.650 | 16.0 ± 1.9 |
| PM-08 | 53.9316 | 16.2611 | 75 | 3.2 | 1.0000 | 21.56 | 7.723 ± 0.656 | 17.3 ± 2.0 |
| PM-09 | 53.9072 | 16.7199 | 174 | 2.8 | 0.9994 | 17.60 | 8.678 ± 0.687 | 17.6 ± 1.9 |
| PM-10 | 53.9576 | 16.7262 | 181 | 1.2 | 0.9874 | 8.98 | 9.228 ± 0.690 | 18.5 ± 2.0 |
| PM-11 | 54.0496 | 16.4278 | 100 | 3.5 | 0.9630 | 21.54 | 8.011 ± 0.552 | 18.2 ± 1.9 |
| PM-12 | 54.1706 | 16.8343 | 119 | 1.4 | 1.0000 | 19.36 | 10.222 ± 0.572 | 21.6 ± 2.0 |
| PM-13 | 54.1909 | 16.7664 | 110 | 1.2 | 0.9994 | 20.57 | 7.799 ± 0.454 | 16.6 ± 1.6 |
| PM-14 | 54.1860 | 16.7453 | 113 | 3.8 | 1.0000 | 19.06 | 7.116 ± 0.403 | 15.4 ± 1.5 |
| PM-15 | 54.1770 | 16.7886 | 115 | 2.3 | 1.0000 | 22.92 | 6.872 ± 0.521 | 14.7 ± 1.6 |

| | | | | | | | | |
|---|---|---|---|---|---|---|---|---|
| PM-16 | 54.2823 | 17.1412 | 137 | 1.7 | 1.0000 | 16.42 | 9.279 ± 1.044 | 19.3 ± 2.6 |
| PM-17 | 54.2883 | 17.9010 | 248 | 2.6 | 0.9996 | 19.83 | 10.965 ± 0.512 | 20.5 ± 1.8 |
| *PM-20* | *54.4242* | *18.0064* | *192* | *2.0* | *1.0000* | *21.34* | *21.886 ± 2.205* | *43.2 ± 5.5** |
| **Vistula Ice Stream area** | | | | | | | | **17.0 ± 0.8** |
| POM-1 | 53.7236 | 19.7514 | 99 | 1.0 | 1.0000 | 72.519 | 9.210 ± 0.630 | 20.7 ± 2.1 |
| POM-2 | 53.8444 | 19.8236 | 107 | 2.0 | 1.0000 | 70.065 | 6.810 ± 0.480 | 15.3 ± 1.6 |
| PM-19 | 53.9621 | 18.3522 | 112 | 1.9 | 0.9872 | 13.84 | 8.979 ± 0.691 | 19.4 ± 2.1 |
| *PM-24* | *54.4910* | *18.2682* | *192* | *2.4* | *1.0000* | *24.57* | *15.598 ± 0.876* | *30.8 ± 2.9** |
| PM-25 | 54.5126 | 18.2352 | 206 | 1.2 | 1.0000 | 19.96 | 8.068 ± 0.475 | 15.5 ± 1.5 |
| PM-26 | 54.5465 | 18.3146 | 170 | 1.9 | 1.0000 | 25.60 | 9.019 ± 1.221 | 18.1 ± 2.8 |
| PM-27 | 54.5038 | 18.2681 | 200 | 2.5 | 0.9939 | 27.62 | 7.659 ± 0.423 | 15.1 ± 1.4 |
| PM-28 | 54.1910 | 18.4396 | 188 | 3.8 | 1.0000 | 20.92 | 6.388 ± 0.471 | 12.8 ± 1.4 |
| PM-29 | 54.1910 | 18.4396 | 188 | 2.4 | 1.0000 | 18.34 | 9.006 ± 0.514 | 17.9 ± 1.7 |
| *PM-30* | *54.3006* | *18.4038* | *166* | *2.1* | *0.9997* | *20.96* | *12.482 ± 0.912* | *25.3 ± 2.7** |
| PM-31 | 54.3932 | 18.5100 | 109 | 4.2 | 1.0000 | 22.11 | 8.336 ± 0.550 | 18.2 ± 1.8 |
| **Mazury Ice Stream area** | | | | | | | | **16.4 ± 0.3** |
| POM-3 | 54.0861 | 20.9097 | 117 | 2.0 | 1.0000 | 40.005 | 7.92 ± 0.58 | 17.6 ± 1.9 |
| *POM-4* | *53.9569* | *20.8597* | *167* | *1.5* | *1.0000* | *70.132* | *5.95 ± 0.42* | *12.5 ± 1.3** |
| POM-5 | 53.9006 | 21.2028 | 175 | 2.0 | 1.0000 | 69.995 | 7.34 ± 0.61 | 15.4 ± 1.7 |
| POM-8 | 54.0681 | 21.6097 | 138 | 3.0 | 1.0000 | 57.034 | 7.43 ± 0.65 | 16.3 ± 1.9 |
| POM-10 | 54.1500 | 21.9958 | 173 | 1.0 | 1.0000 | 40.134 | 6.88 ± 0.55 | 14.3 ± 1.6 |
| POM-11 | 53.9006 | 22.0167 | 177 | 1.0 | 1.0000 | 55.301 | 7.73 ± 0.53 | 16.0 ± 1.6 |
| POL-1 | 53.7739 | 21.6286 | 117 | 2.0 | 1.0000 | 30.175 | 7.90 ± 0.71 | 17.6 ± 2.1 |
| POL-1B | 53.7739 | 21.6286 | 117 | 2.0 | 1.0000 | 30.021 | 7.17 ± 0.85 | 16.0 ± 2.2 |
| POL-wm^ | | | | | | | | 16.9 ± 1.7 |
| POL-2 | 54.2147 | 21.8589 | 128 | 2.0 | 1.0000 | 30.861 | 7.71 ± 0.64 | 16.9 ± 1.9 |
| *POL-3* | *54.1950* | *21.9464* | *130* | *2.0* | *1.0000* | *29.988* | *11.97 ± 1.04* | *26.3 ± 3.0** |
| POL-4 | 54.2358 | 22.7897 | 240 | 2.0 | 1.0000 | 30.267 | 8.39 ± 0.71 | 16.5 ± 1.9 |
| POL-4B | 54.2358 | 22.7897 | 240 | 2.0 | 1.0000 | 20.227 | 9.64 ± 1.14 | 18.9 ± 2.7 |
| POL-4wm^ | | | | | | | | 17.2 ± 1.7 |

| | | | | | | | | |
|---|---|---|---|---|---|---|---|---|
| POL-5 | 54.2039 | 22.7531 | 243 | 2.0 | 1.0000 | 30.180 | 8.32 ± 0.72 | 16.3 ± 1.9 |
| POL-5B | 54.2039 | 22.7531 | 243 | 2.0 | 1.0000 | 30.046 | 10.25 ± 1.22 | 20.1 ± 2.8 |
| POL-5wm^ | | | | | | | | 17.3 ± 1.7 |
| *POL-6* | *54.1647* | *22.9683* | *211* | *2.0* | *1.0000* | *28.208* | *41.06 ± 3.07* | *84.0 ± 9.1** |
| POL-7 | 54.1642 | 22.9700 | 195 | 2.0 | 1.0000 | 30.066 | 10.10 ± 0.83 | 20.7 ± 2.3 |
| POL-7B | 54.1642 | 22.9700 | 195 | 2.0 | 1.0000 | 22.092 | 9.86 ± 1.00 | 20.2 ± 2.6 |
| *POL-7wm^* | | | | | | | | *20.5 ± 1.9** |
| **Riga Ice Stream area** | | | | | | | | **15.5 ± 0.5** |
| BALTI-2 | 55.698 | 25.799 | 113 | 3.5 | 1.0000 | 52.864 | 6.72 ± 0.50 | 15.1 ± 1.6 |
| BALTI-3 | 55.310 | 25.431 | 142 | 2.0 | 1.0000 | 69.716 | 7.41 ± 0.55 | 16.0 ± 1.7 |
| BALTI-4 | 55.434 | 25.509 | 167 | 2.0 | 1.0000 | 60.775 | 7.84 ± 0.64 | 16.5 ± 1.8 |
| BALTI-5 | 55.494 | 25.657 | 154 | 2.0 | 1.0000 | 49.123 | 6.19 ± 0.47 | 13.2 ± 1.4 |
| LIT-2 | 55.544 | 25.846 | 187 | 2.0 | 1.0000 | 30.003 | 8.31 ± 0.73 | 17.1 ± 2.0 |
| LIT-3 | 55.544 | 25.846 | 187 | 2.0 | 1.0000 | 29.995 | 7.55 ± 0.68 | 15.6 ± 1.8 |
| LIT-3B | 55.544 | 25.846 | 187 | 2.0 | 1.0000 | 30.434 | 9.70 ± 1.24 | 20.0 ± 3.0 |
| LIT-3wm^ | | | | | | | | 16.6 ± 1.7 |
| LIT-8 | 54.273 | 24.021 | 190 | 3.8 | 1.0000 | 70.062 | 7.02 ± 0.56 | 14.7 ± 1.6 |
| LIT-9 | 54.520 | 24.315 | 176 | 2.6 | 1.0000 | 48.370/ | 7.09 ± 0.54 | 14.9 ± 1.6 |
| **Novgorod Ice Stream area** | | | | | | | | **14.7 ± 0.5** |
| BEL-13 | 55.658 | 27.683 | 151 | 2.8 | 1.0000 | 71.447 | 7.18 ± 0.70 | 15.5 ± 1.9 |
| BEL-14 | 55.639 | 27.375 | 150 | 1.7 | 1.0000 | 71.029 | 6.19 ± 0.47 | 13.2 ± 1.4 |
| BEL-15 | 55.699 | 26.994 | 144 | 0.5 | 1.0000 | 29.117 | 6.99 ± 0.62 | 14.9 ± 1.7 |
| BEL-15A | 55.699 | 26.994 | 144 | 0.5 | 1.0000 | 34.198 | 7.39 ± 0.62 | 15.7 ± 1.8 |
| BEL-16 | 55.544 | 27.076 | 152 | 2.0 | 1.0000 | 70.022 | 6.63 ± 0.46 | 14.2 ± 1.5 |

Samples MVP, BER, POM, PM, POL, BALTI, LIT and BEL measured at the ASTER facility (Rinterknecht et al, 2006; this study). Samples SJAE, FYN and JYL measured at the SUERC AMS Laboratory (Houmark-Nielsen et al., 2012). Samples PO measured at the PSI/ETH Zürich tandem accelerator facility (Heine et al., 2009). AMS $^{10}Be/^{9}Be$ results are standardized to NIST SRM 4325 (samples POM, POL, BALTI, LIT, BEL, SJAE, FYN and JYL), STD-11 (samples MVP, BER, PM) and S555 (samples PO) standards. $^{10}Be/^{9}Be$ ratios were corrected for a process blank values of $3.8 \times 10^{-15}$ (samples POM, POL, BALTI, LIT, BEL), $1.3 \times 10^{-15}$ (samples MVP), from 2.9 to $13.2 \times 10^{-15}$ (samples SJAE, FYN and JYL) and $4.44 \times 10^{-15}$ (samples PM). Exposure ages were calculated using a standard atmosphere and a rock density of 2.7 g $cm^{-3}$.

[1] Corresponding to self-shielding (direction and angle of surface dip).
^error-weighted mean age of two samples taken from one boulder.
*surface exposure ages not used (outliers) in calculation of the arithmetic mean with the standard deviation of the mean (italic).
n.a. – not available.

Table 2. Radiocarbon dates significant for constraining the minimum age of ice retreat from the PP ice-marginal belt. The conventional $^{14}C$ ages were calibrated with OxCal 4.4 according to *IntCal20* calibration curve (Reimer et al., 2020).

| **Sample** | **Site** | **Dated material** | **Stratigraphic context** | **Method** | **$^{14}C$ age [yr BP]** | **Calibrated age [cal ka BP]** | **References** |
|---|---|---|---|---|---|---|---|
| Ua-1023 | Nivå (section) | bone | Late Glacial lacustrine deposits | AMS | 14 100 ± 300 | 17.16 ± 0.44 | Lagerlund and Houmark-Nielsen (1993) |
| Gd-15891 | Rega River (section) | carbonate | Late Glacial gyttja | conv. | 14 430 ± 150 | 17.63 ± 0.23 | Gliwice Radiocarbon Database (GRDB) |
| Gd-15907 | Rega River (section) | carbonate | Late Glacial gyttja | conv. | 16 450 ± 260 | 19.88 ± 0.32 | Gliwice Radiocarbon Database (GRDB) |
| Gd-12636 | Jasień Lake (core) | organic | Late Glacial gyttja | conv. | 13 360 ± 240 | 16.10 ± 0.36 | Gliwice Radiocarbon Database (GRDB) |
| Gd-6311 | Boże Pole (section) | organic | Late glacial peat | conv. | 13 010 ± 220 | 15.58 ± 0.34 | Błaszkiewicz (1998) |
| Gd-10818 | Stary Cieszyn (core) | organic | Late Glacial peat | conv. | 13 420 ± 220 | 16.19 ± 0.33 | Niewiarowski (2003) |
| GdA-137 | Miłkowskie Lake (core) | plant macrofossil | Late Glacial lacustrine deposits | AMS | 13 960 ± 100 | 16.95 ± 0.17 | Czernik (2009) |
| KIA33887 | Hańcza Lake (core) | wood | Late Glacial lacustrine deposits | AMS | 12 220 ± 45 | 14.15 ± 0.11 | Lauterbach et al. (2011) |
| Poz-35959 | Linówek Lake (core) | seeds | Late Glacial lacustrine deposits | AMS | 11 690 ± 60 | 13.87 ± 0.10 | Gałka and Sznel (2013) |
| n.a. | Bebrukas Lake (core) | organic | Late Glacial peat/gyttja | conv. | 11 800 ± 300 | 13.80 ± 0.41 | Neustadt (1977) |
| Mo-205 | Vievis bog (core) | organic | Late Glacial peat | conv. | 11 200 ± 340 | 13.14 ± 0.35 | Serebryanny (1978) |

n.a. – not available.